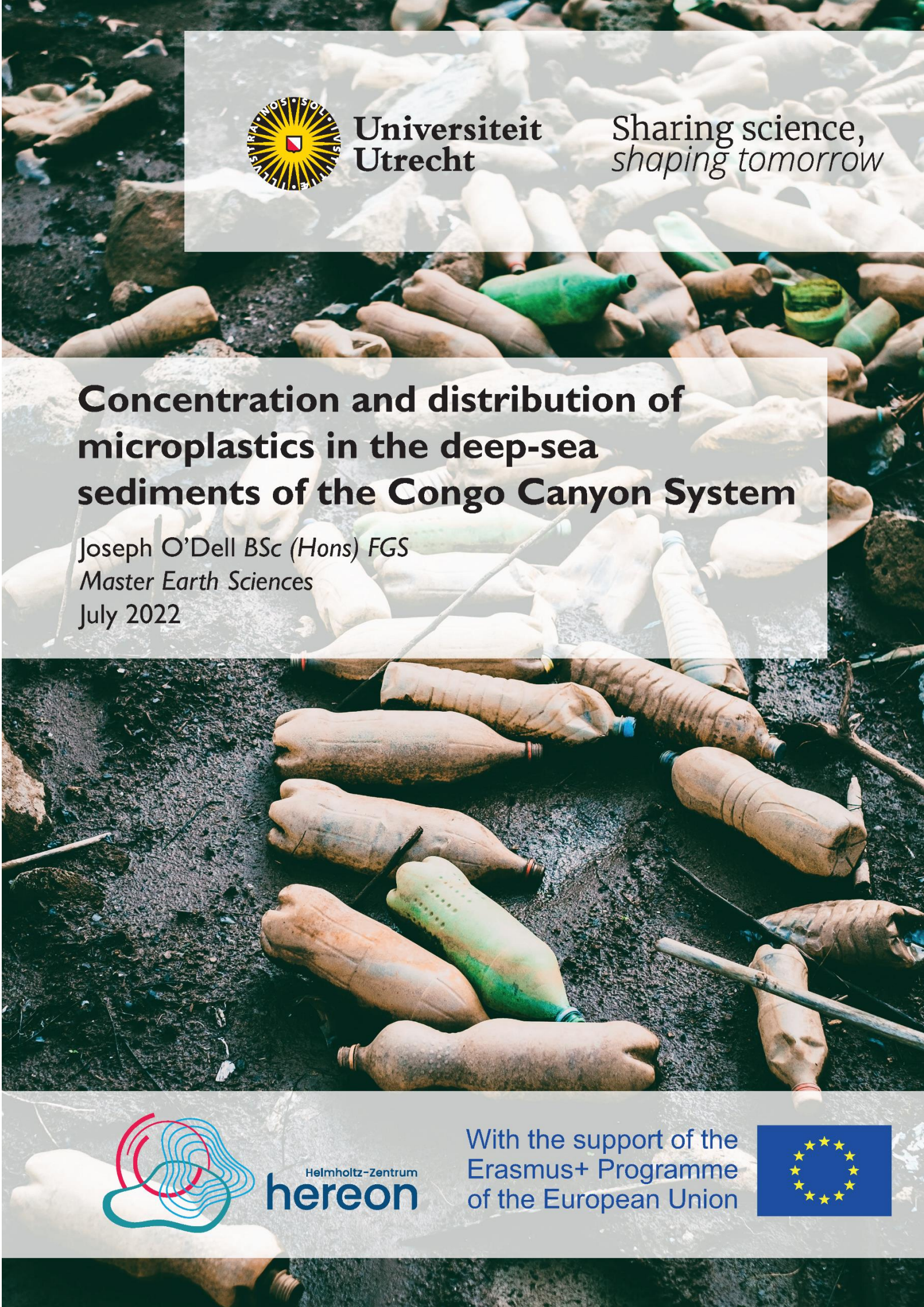

Universiteit Utrecht

Sharing science, *shaping tomorrow*

Concentration and distribution of microplastics in the deep-sea sediments of the Congo Canyon System

Joseph O'Dell *BSc (Hons) FGS*
Master Earth Sciences
July 2022

Helmholtz-Zentrum hereon

With the support of the Erasmus+ Programme of the European Union

Utrecht University

Sharing science,
shaping tomorrow

Concentrations and distribution of microplastics in the deep-sea sediments of the Congo Canyon System

Joseph O'Dell BSc (Hons) FGS

Master of Science in Earth Sciences

Integrated Stratigraphy and Sedimentary Systems Track

Utrecht University

July 2022

Supervisors

Dr. Florian Pohl

Marine Litter Unit, University of Plymouth, GB

Dr. Joris T. Eggenhuisen

Department of Earth Sciences, Utrecht University, NL

Dr. rer. nat. Daniel Pröfrock & Dr. Lars Hildebrandt

Inorganic Environmental Chemistry, Helmholtz-Zentrum hereon GmbH, DE

Table of Contents

List of Figures

List of Tables

Disclaimers

Statement of originality of the MSc thesis

I, Mr. Joseph O'Dell, declare that:

1. this is an original report, which is entirely my own work,

2. where I have made use of the ideas of other writers, I have acknowledged the source in all instances,

3. where I have used any diagram or visuals, I have acknowledged the source in all instances,

4. this report has not and will not be submitted elsewhere for academic assessment in any other academic course.

Name: Joseph O'DELL

Registration number: 6678513

Date:

Signature:

Erasmus+ grant

The European Commission's support for the production of this publication does not constitute an endorsement of the contents, which reflect the views only of the authors, and the Commission cannot be held responsible for any use which may be made of the information contained therein.

Author's remarks

Citations & style

The following report is written in British English, following the author's mother tongue. In line with the developments in academic literature, this is written in both active and passive form. Citations are given in the style of Journal of the Geological Society of London.

Acknowledgements

The amazing support and kindness of Doris Schnalke, Andrea Pieper, Catharina Petrauskas, Ole Klein, and Anne Hartlich of the Helmholtz-Zentrum-Hereon in Geesthacht, Germany is greatly appreciated and was instrumental in the execution of my project.

Rebecca Aveson, Henk-Jan Geurts, and Josephien Lingbeek extremely generously provided detailed feedback, comments, and improvements on the report and presentation.

Robert Lanson Arklay and Dr. Claire Dyer take the blame for introducing me to rocks in the first place, and Dr. Dean Bullen for putting up with me during my bachelors.

Foreword

Plastic. One word, seven broad categories, and an almost-infinite combination of chemicals and manufacturing techniques. Its omnipresence was previously seen as a success, and we as humans lauded it for its applicability as a miracle material. Plastic now dominates our lives, coming smothered around every new purchase and protecting us from the unknown.

While the widespread use of plastic products in society has increased greatly since World War 2, our thinking and understanding of the processes that manage the waste, including what happens when plastic breaks down, have been so far stunted. But we now know that is also intruding into our food networks, via our rivers and waterways, and primarily due to the fact that the management culture for our 'single use society' has failed to responsibly reduce, reuse, and recycle plastic waste.

Sedimentology, which originally uses skills designed for timescales in the millions of years, can help unlock as to where the plastic that enters our rivers and seas 'goes'.

Abstract

Turbidity currents are underwater flows of sediment, and a major process in the distribution of sediment. Submarine canyon systems can stretch for hundreds, if not thousands of kilometres out into the deep ocean. They offer a timeline of sedimentary process, and additionally act as record keeper for our pollution of the rivers and seas.

The Congo Canyon is a submarine canyon system off the coast of the Democratic Republic of the Congo, Western Africa with a proximal part in the territorial waters of Angola. Submarine events in the canyon can last weeks and may result in the transport of numerous cubic kilometres of sedimentary material. However, we do not currently know for certain that these events transport plastic, nor how much material they transport.

In this project I processed collected cores sediments from the Congo Canyon to remove organic material and isolate microplastics. I analysed them using LD-IR (Laser Direct Infrared Spectroscopy) following the technique developed by the Helmholtz-Zentrum Hereon to determine the presence, frequency, and polymer classification of each sample.

Plastics were ubiquitous amongst all of the core samples, and my calculations showed that up to 9,138 microplastic particles per kilogram of sediment were present in the Congo Canyon System. I did not find that grain size impacted the sorting or dispersal of microplastic fragments, however the density of the polymer resulted in preferential deposition, where higher density plastics were deposited earlier in the channel.

However, I acknowledge the size of this dataset, and that further interlinking with sediment trap data is required to understand the input of sediment from the water column. I have made recommendations on future lab work, possible refinements to the lab protocol, and additional validation of the current process to further strengthen the applicability of this work.

Introduction

We require and consume more and more 'things' in our lives. Whether made of it, or wrapped in it, plastic is so fast evolving that Bakelite, the first truly synthetic plastic produced by Leo Hendrik Bakeland PhD (1863-1944), is almost unrecognisable compared to the diversity of today's plastics.

To many of us, plastic is just one word, but covers many different families and groupings of materials; A "plastic" bag may be made from (linear) low density polyethylene ([L]LDPE) or polytetrafluoroethylene (PTFE or Teflon®) amongst many other possibilities. And 'polystyrene' ranges from rigid, brittle enclosures for electronics (polystyrene [PS]) to disposable lightweight takeaway food containers (expanded polystyrene [EPS]).

Geyer *et al.* (2017) estimated that over 8300 million metric tons of virgin plastic had ever been produced between 1950 to 2015, with the annual production growing exponentially. The consumption of plastic across so many sectors results in an almost unfathomable rate of use and disposal, and as of 2015 an estimated 6300 Mt had become waste. 79% of that waste could not be accounted for in recycling or incineration systems, and so was assumed to have been disposed in landfill or to have accumulated in the natural environment. Not every single piece of this plastic waste remained in situ, and so plastic pollution is not a problem that is going to go away any time soon.

As a result of high demand for plastic products in both consumer and commercial systems, coupled with poor waste processing networks, vast quantities of plastic material enter the ocean - estimated running total up was 4.8 – 12.7 million Mt up to 2015 alone (Jambeck *et al.* 2015; Geyer *et al.* 2017). This plastic waste is very diverse in terms of its size, shape, and polymer type.

Despite the stability of plastics as a material, they are still subjected to degradation, primarily by sunlight. Figure 1 shows the example of a plastic bottle, that as time progresses is exposed to heat, cold, sunlight, and mechanical erosion as it rustles in the wind and high water. These stresses result in the weakening of the bonds in the polymer, and the bottle is fractured into smaller particles (Figure 1). If these particles are smaller than 5mm, they are defined as microplastics, following both the definition of the National Oceanographic and Atmospheric Administration from 2008 (Arthur *et al.* 2008) as well as additional studies

(Verschoor 2015; Hartmann *et al.* 2019). The smaller the microplastics are, the easier they can be transported away by wind or water.

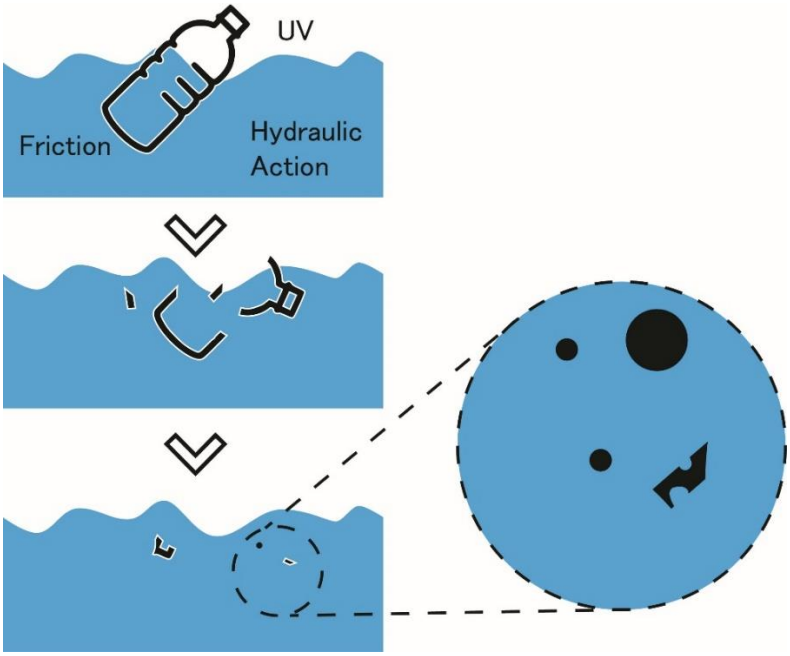

Figure 1 - Graphic representation of breakdown of a plastic bottle to microplastics

In addition, microplastic may also be primary produced products, such as microbeads manufactured by the cosmetics industry. Concerningly, microplastics are eventually taken up by marine organisms and result in both physical and potential toxin contamination of the food web (von Moos *et al.* 2012; Cole *et al.* 2013; Verschoor 2015; Lim 2021).

A continuation of the plastic breakdown process might lead to particles that reach the limits of detectability and the boundary where particles could be freely taken up in the blood stream (Kwon *et al.* 2022). These very small plastic particles are also known as nanoplastics. To this end, the IUPAC recommended in 2011 a lower size limit for microplastics of 0.1 µm, and nanoplastics defined in the range 0.0001 – 0.1 µm (Slomkowski *et al.* 2011). However due to technological innovations, including the development of the Laser Direct Infrared (LDIR) spectral imaging apparatus used in this project, the lower size limit should be set at a lower value of 10 µm (see Hartmann et al. 2019 for a review on plastic size definitions).

First discovery of marine plastic pollution

The first published report on plastic contamination in the sea by Carpenter and Smith (1972) can be considered as the first realisation of marine plastic pollution. They noticed that every floating debris net they launched in the Sargasso Sea (an area of the Atlantic Ocean west of Bermuda, bounded by ocean currents) returned with plastic contamination.

At the time of their work in 1972 they presumed that these particles mostly acted as a growth surface for organisms such as bacteria, however Carpenter & Smith did also consider other contemporary ideas that the polychlorinated biphenyls (PCBs) used as a plasticiser could be released from these plastics during breakdown and bioaccumulate in marine organisms (Harvey *et al.* 1971).

I consider this to be the starting point of not only modern microplastic research, but also for the whole system thinking of plastic and the products of their breakdown.

Modern day

Despite the figurative sea of pollutants building up around the world, modern research into plastic pollution and microplastics has reached the forefront only within the past two decades. Gross (2015) states that:

> *"Plastic pollution of the oceans is a growing problem about which far too few details are known with any certainty"*

This appears reflected in the public psyche, with the release of the well-recognised documentary film 'A Plastic Ocean' (Leeson 2016) marking the beginning of a period of heightened, and somewhat renewed interest in the subject.

Recent research indicates that microplastic pollution is now not only an environmental issue, but a public health issue, defining plastics as 'potentially hazardous substances in animals' due to the ability of test nanoplastic particles of 0.2 – 1.0 μm to trigger programmed cell death (*microglial apoptosis*) in subject animals. (Kwon *et al.* 2022)

Further, plastic pollution results in problems with water quality, aquatic life, and the sustainability of the ecosystem services provided by the hydrological environment. However, microplastics are of further interest due to the pervasive impact – not only within the food web, but also into the sedimentary record.

Deep marine canyons

Deep, or sub-marine canyons are commonly, but not exclusively located along active continental margins and are generally associated large rivers which input vast quantities of suspended sediment (Hay 2016). Rivers are primary sedimentary transport methods, being themselves not only rich in sediments but also (in)organic matter (Costa 2016). Sediments accumulate in a wedge at the mouth of the river as velocity decreases at the confluence with the ocean and suspended matter stops being mobilised.

The sediments which have accumulated on the wedge at the end of the fluvial channel (Figure 2, red zone) are then triggered either through overloading or through a seismic event to mobilise, which results in a large deluge of suspended sediment and (in)organic material flowing through gravitational pull towards the ocean floor, forming a low-viscosity flow of mixed grains supported by fluid turbulence, known as a turbidity current (Stow 1994; Selley 2000).

The large influx of water and sediment forms the canyons as they flush through a topographically complex deep offshore (Figure 2, light blue & green zones), and incises into the continental slope to form levee-banked channels (Figure 2, dark blue zone). Incision of these levee banked channels into the continental slope can be up to 2km deep (Hay 2016).

Turbidity currents are rapid, downhill flows of water caused by an increased density due to large volumes of sediment. They travel at high speed, and can endure up to a week while moving enormous quantities of sediment (Azpiroz-Zabala *et al.* 2017a, b) and entrain large amounts of additional material as they progress. Due to the enormous volume of material transported, turbidity currents are widely believed to be major contributors to transport and deposition of global sedimentary cover (Selley 2000), especially sand (Shepard 1951). Estimations by Talling *et al.* (2022) indicate that a single event in the Congo Canyon moved between 1 and 2 km^3 of sediment, inclusive of suspended material.

Canyon systems can extend by great distance into the sea, such as the Mona Canyon at 140 km (Gardner *et al.* 1980), and the Northwest Atlantic Mid-Ocean Channel at 3,800 km (Klaucke *et al.* 1998) . The distal deposits at the end of canyon systems are known as deep-sea fans (far reaching channel lobes). Deep sea lobes are of particular geological interest as they act as reservoirs for natural resources including rare earth materials (Garzanti *et al.* 2021), but also retain large quantities of organic matter (Azpiroz-Zabala *et al.* 2017a;

Cantwell 2020; Zhong and Peng 2021) and therefore by extension, may be reservoirs of man-made materials, including microplastics

Turbidity currents are highly energetic flows which makes recording of their flow rates and speed difficult, as deployed sensors are often wiped-out along with the sediment however recorded data shows that flows can endure for up to a week (Azpiroz-Zabala *et al.* 2017b). These environments therefore provide a burial pathway for plastic material that exits a fluvial system, and for which no current final destination can be ascribed to.

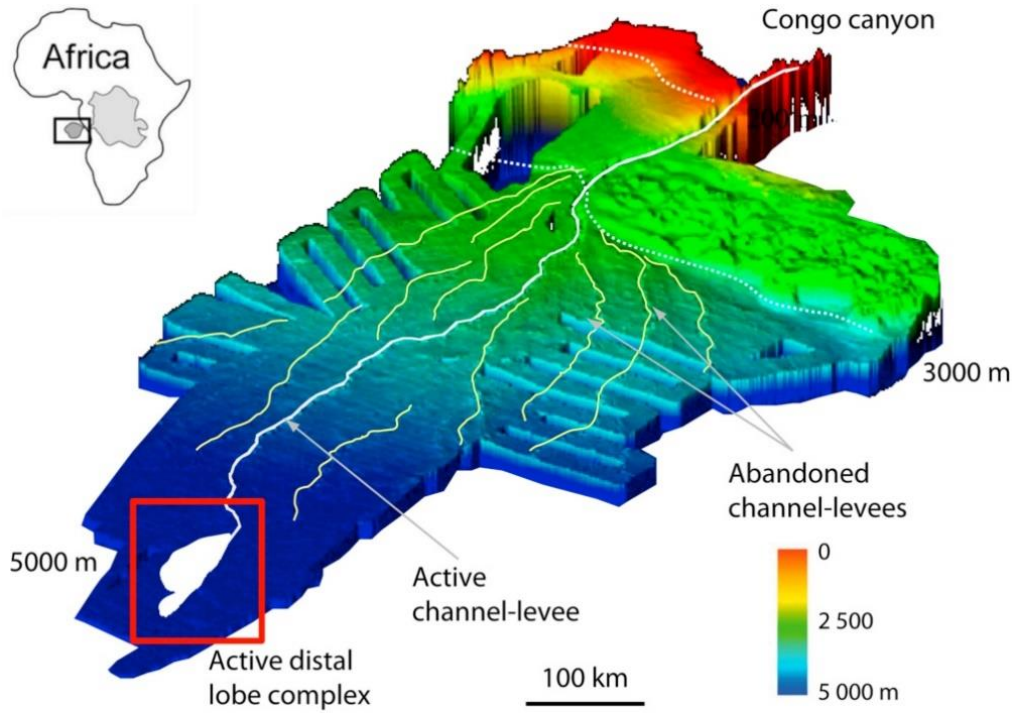

Figure 2 - 3D bathymetric map of the Congo Canyon system, Dennielou et. al. (2017) **after Savoye et. al.** (2009)

Other work in canyon systems

The UN Environmental Programme has acknowledged marine litter to be a key target of the Regional Seas Programme, and as such there is extensive work on the impact of marine litter on the ecosystems in deep sea canyons. This works two fold, initially considering the introduction of material into the deep sea canyon, where it has been shown that canyons act as conduits for anthropogenic (i.e. human, land-sourced) plastic waste and direct this plastic waste to the sea floor (Pierdomenico *et al.* 2019; Zhong and Peng 2021), but also that benthic waste can be dragged along by the sedimentary flows due to their energy levels (Kane *et al.* 2020).

Furthermore, the reworking and distribution of microplastics within a canyon has been evaluated, as the impact of microplastic on deep sea organisms, as well as their interaction with the sedimentary layers in the system is altered through the presence of microplastics (Jones *et al.* 2022) which ultimately can result in additional sequestration of microplastic particles in the sedimentary layers, however microplastics have been shown to inhibit bioturbation of layers (Coppock *et al.* 2021).

Study area – Congo Canyon System

The Congo Canyon (Figure 2) is a well-studied deep sea canyon system, located in the Atlantic Ocean, directly west offshore of the Democratic Republic of Congo, West Africa. The system is directly connected to and fed by the Congo River. It is of particular interest as it is one of the largest and most active canyon systems currently known of (Azpiroz-Zabala *et al.* 2017a)

It is generally unknown how organic matter and microplastics are transported in and deposited by turbidity currents (Dennielou *et al.* 2017; Pohl *et al.* 2020). Kane and Clare (2019) proposed that variation in flow velocities and durations may influence the sorting of the plastic fragments in the flow and the resulting deposit, however they concede that this needs to be validated with data. Flume tank analogues by Pohl *et al.* (2020) indicate that our current understanding of these flows is not sufficient to fully explain observed transport processes and depositional patterns of different microplastics by turbidity currents.

The concentration of microplastic fibres in the deposits is larger than at the base of the flow, suggesting a distinctly different depositional mechanism for microplastic fibres leading

to their enrichment in the deposits. Pohl *et al.* (2020) further states that the transport behaviour of plastics in deep sea flows is not yet fully possible to define based on our current understanding of these flows.

Enders *et al.* (2019) propose that the sediment grain size is inherently linked to the load of microplastics in a sedimentary system and even suggest grain size as a *'critical proxy'*. Their research implies that there is a link between the sediment grain size and the density of the plastic polymers. As such, the concentration of high density polymers increases with the sand content, and the overall concentration of polymers increases with the content of fine sediments (Enders *et al.* 2019).

Despite the knowledge that deep sea sedimentary flows can trap microplastics, and that there are plastics in the Kinshasa River (Ocamringa 2021), and therefore the Congo Canyon, the location and quantity of microplastics in the Congo deep sea system. Therefore, I believe analysis of the sediments is required to expand our understanding of the behaviour and deposition of plastics in the sedimentary record.

Research questions

The purpose of my MSc thesis project is to analyse sediment cores from the Congo Canyon, Democratic Republic of the Congo & offshore Angola, Western Africa to determine the distribution of plastics in the canyon and further into the fan.

I will combine the microplastic analysis of the material with understandings of the sedimentary environment, characteristics of the pollutants, and the possible routes of transfer into the deep-sea system.

I seek to answer the following questions through this project;

- What is the variation in microplastic concentration, size, shape, and polymer-type across different sub environments of the Congo Canyon System?
- Does the microplastic distribution correlate with the sediment grain size?
- What are the possible causes for the distribution pattern of microplastics in a submarine canyon system and could these variations be explained with sediment transport processes?

Dataset and sample selection

20 cores were collected from the Congo Canyon on cruise JC187. The cores have already been subsampled and freeze-dried at the University of Durham, UK and are stored at the Helmholtz-Zentrum Hereon (Geesthacht, Germany).

Out of the available samples, we select fifteen for microplastic analysis. Our selection process for the samples considers:

- Bathymetric maps and cross-sections provided by the cruise report to determine depositional environment
- Viability of sample for analysis (sufficient volume)
- Core grain size using preliminary grain size data
- Samples providing comparison across a transect of the canyon system (e.g., comparing terrace and channel thalweg deposits)
- Comparing microplastic contamination in distal and proximal areas of the canyon system
- The youngest (top) of the core will be used to yield the most recent deposits, and therefore the most likely to contain plastics.
- Contrast between sandy (D_{50} > 50 µm) and muddy/silty (D_{50} < 50 µm) layers to enable better understanding of retention of microplastic in sand-loaded sediments

In total I will process fifteen samples as detailed in the sample table (Table 1)

Cores with a grain size above 50 µm are preferentially chosen as they indicate a higher sand content following the logic given above, however only 3 samples with a grain size above 50 µm are suitable.

Cruise outline

A series of research cruises have been defined, with cruise JC187 being conducted under the guidance of Peter J Talling (Department of Geography, University of Durham, UK) using vessel RRS James Cook from the National Oceanography Centre Southampton (NOCS), UK. She departed from Mindelo, Cape Verde, Macaronesia on Saturday 31st August 2019 and returned to Walvis Bay, Namibia, Africa on Monday 7th October 2019[1].

The overall programme of cruises, of which JC187 was the first, aims to deploy moored sensors for a four-year period to determine the sediment flow physical properties, and additionally multi-cores were collected along the stations to provide both content for microplastic analysis as well as basin stratigraphic analysis. Multi-beam surveys were also conducted at two sections, first in the international water section of the channel and secondly in the upper canyon.

[1] Cruise report available at https://www.bodc.ac.uk/resources/inventories/cruise_inventory/report/17243/

Table 1 - List of samples

Core ID	Sample	Environment	Distance from Shore (km)	Reason
MC-02 B	S_07	Lobe	754.05	Compares plastic preservation from top and middle of core.
MC-02 C	S_08	Lobe		
MC-03 B	S_31	Terrace	691.04	Very distal channel deposit, these two provide comparison between preservation in the same location but in different environments.
MC-04 B	S_33	Thalweg	689.73	
MC-05 B	S_11	Thalweg	140.58	Distal thalweg deposit, these two provide comparison between preservation in the same location but in different environments.
MC-07 B	S_15	Terrace	140.85	
MC-08 A	S_04	Thalweg	107.49	Compares to MC-08 B performed by Florian Pohl, validates picking of top of core.
MC-10 B	S_24	Terrace	107.33	Thalweg deposit, these two provide comparison between preservation in the same location but in different environments, plus comparison against MC-08 A (same location)
MC-11 B	S_26	Terrace	106.85	
MC-12 B	S_28	Terrace	97.56	Channel thalweg deposit, these two provide comparison between preservation in the same location but in different environments.
MC-13	S_16	Thalweg	96.28	
MC-16 B	S_35	Thalweg	91.19	Comparison of Thalweg preservation against other samples
MC-21	S_29	Thalweg	128.28	Preservation of energy at a high energy meander bend transect
MC-24 B	S_19	Terrace	460.27	Compares preservation in the terrace in the very distal submarine channel (400km downstream)
MC-25 C	S_22	Out of Canyon	458.51	Comparison of out of canyon deposits versus in canyon deposits

Method

Microplastic separation

The sediment cores were collected from the Congo Canyon on the research vessel and were mostly comprised of siliciclastic sediment with organic matter. I needed to isolate the microplastics from the sediments as well as from organic material to be analysed. After separation, I transferred microplastic particles to a glass slide and analysed them using Laser Direct Infrared Spectroscopy (LDIR).

The initial lab work protocol was developed at the Helmholtz-Zentrum Hereon (Hildebrandt *et al.* 2020, 2021; El-Gareb 2021) outlined a seven-stage processing procedure to take sediment core sub-samples and remove the majority of the siliciclastic material for imaging.

General working procedure

I rinsed all glassware with 96% Ethanol, then 30% Ethanol, and MilliIQ water to remove possible contamination from storage, transport, or from settling out of the laboratory air. After rinsing, glassware was then stored in a clean flow bench prior to use. Equipment that I used multiple times for various samples (e.g., tweezers, funnels) is rinsed in the same fashion, but also rinsed within the clean bench following the same process between uses.

The laboratory stored reagents in brown glass bottles with FEP (Nalgene) stoppers, which I also flushed following the protocol above. All reagents were filtered over 0.4 µm polycarbonate filters, except Zinc Chloride which I double filtered over 1.2 µm glass fibre.

Petri dishes, stopper bottles, and MirrIR slides were held at 250 degC in a sterilising oven for 6 hours and then stored in a metal box which had been cleaned with isopropyl alcohol in the clean bench prior to use.

A full list of materials I used in the analysis is provided at Appendix I.

An overview of spectroscopy

Spectroscopy is the use of light at specific wavelengths to excite particles and then measure the relative amount of reflectance or absorbance. A particle is loaded into an apparatus and then subjected to light at a defined range of wavelengths, and the intensity of the response from the particle is recorded.

The reflectance across a range of wavelengths can then be compared to a library of spectra and the similarity of the spectra to the library pattern can be evaluated by the 'hit' or 'match' rate, calculated by the root mean square (regression) between the two spectra. This gives a probable match to the particle, so long as the particle is known in the local library.

Many spectroscopic techniques have been developed and refined, such as Raman spectroscopy which relies on the excitation of particles at a single wavelength, and Fourier-transform infrared spectroscopy (FTIR) which requires direct contact for analysis.

Laser Direct Infrared (LDIR) imaging is an emergent type of spectroscopic imaging technique using a quantum cascade laser (QCL). QCLs were first developed in the 1990's and provide much finer-tuned capabilities for emitting light in specific frequencies (Faist *et al.* 1994), as required by the LDIR. This allows the apparatus to image across the entire spectral range in a faster, automated process.

The centre of the analytical method of my project relies on the use of spectroscopic analysis of particles and comparing them to 'reference' spectra held in a library. In this project I relied on the two microplastic libraries assimilated by the Helmholtz-Zentrum Hereon, namely Hereon MP and Microplastic Starter 1.0. I define the libraries to contain both pure 'reference' spectra, added by the manufacturer and by the laboratory through direct analysis of known particles, and incidental 'local' spectra added by the laboratory during spectral analysis of samples from the same cruise to aid identification of particles in the current working block.

Specifically, in this project I used a Laser Direct Infrared spectroscope (Agilent 8700 LDIR), this operates in a narrower spectral window (1799 – 975 cm^{-1}) than similar spectroscopic technologies, however has numerous benefits due to the spectral resolution and the automatic detection and analysis of particles. (Luo *et al.* 2022)

The LDIR apparatus first scanned each slide at wavelength 1799 cm^{-1} to discriminate particle boundaries. After detection of each particle, the software then targets a focal point of each

particle and performs an automated spot analysis once part particle across the entire slide. These detected spectra are then compared against the reference library to provide the top five based upon root mean squared (also known as the quadratic mean, i.e. the difference in the wavelength profile between reference and particle spectra) which is interpreted as a 'hit rate'. (Hildebrandt *et al.* 2020, 2021)

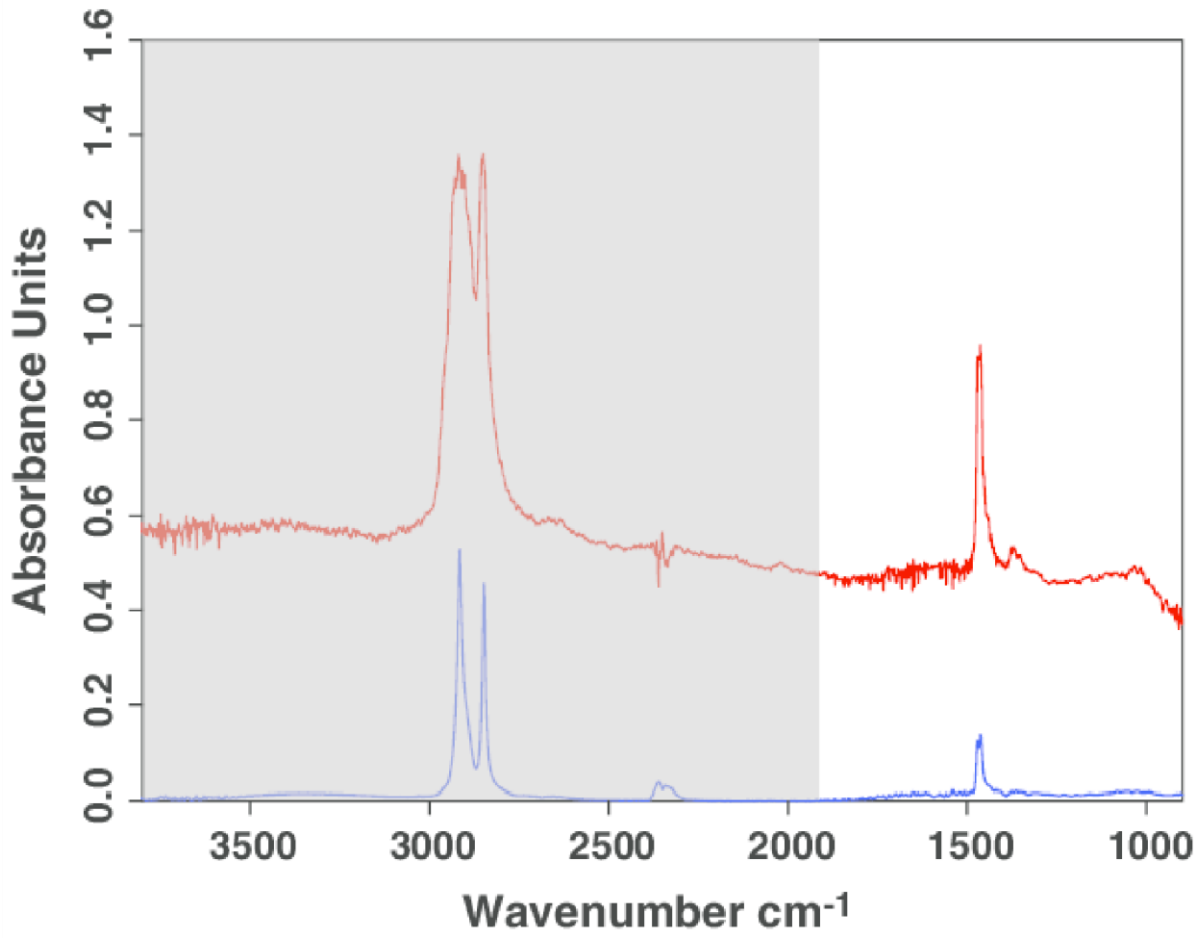

Figure 3 - Example of spectral analysis using example of Polyethylene from Löder & Gerdts (2015), red line is detected spectra, blue line is reference spectra, grey area is unavailable with LDIR technology

Step 1- First Density Separation

In the first step I separated microplastics from the siliciclastic sediment by density separation (e.g. Löder and Gerdts 2015; Coppock *et al.* 2017; López-Rosales *et al.* 2022) (Löder and Gerdts 2015; Coppock *et al.* 2017; López-Rosales *et al.* 2022) where sediment is suspended in a solution of a known density. The central part of the process relies on the fact that the density of Quartz (SiO_2, the major component of siliciclastic sediments) is 2.65 g^{-1} cm^{-3} whilst most plastics were of a lower density (Borges-Ramírez *et al.* 2020). This means that by using a liquid with a specific density between the two end members, I could filter off the lighter particles floated, and the heavier particles sunk and could be removed.

The protocol compiled by the Helmholtz-Zentrum Hereon required the use of Zinc Chloride ($ZnCl_2$) made to a density of 1.7 g^{-1} cm^{-3}, which was pre-prepared by the laboratory. All ground glass parts were lightly lubricated with a medium density silicone grease to improve the quality of the connection and reduce leakage.

30 g of freeze-dried and homogenised sediment was suspended in a glass flask with a PTFE stirring rod and approximately 500 mL $ZnCl_2$, and then connected to a PTFE tap and column. I topped up the suspension with more $ZnCl_2$ to approximately 2/3 of the height of the upper glass module (final volume ZnCl2 750 mL, total volume approximately 800 mL) and sealed with aluminium foil. The tap and column allow for mobilised particles to escape the turbulent zone in the flask and rise to the top of the column (Figure 4).

The stirrer was set to 500 rpm for 24 hours, and afterwards then left to settle for 2 hours, however I checked regularly to ensure that the stirring rod had not become stuck nor was spinning too fast and ejecting denser particles into the upper column.

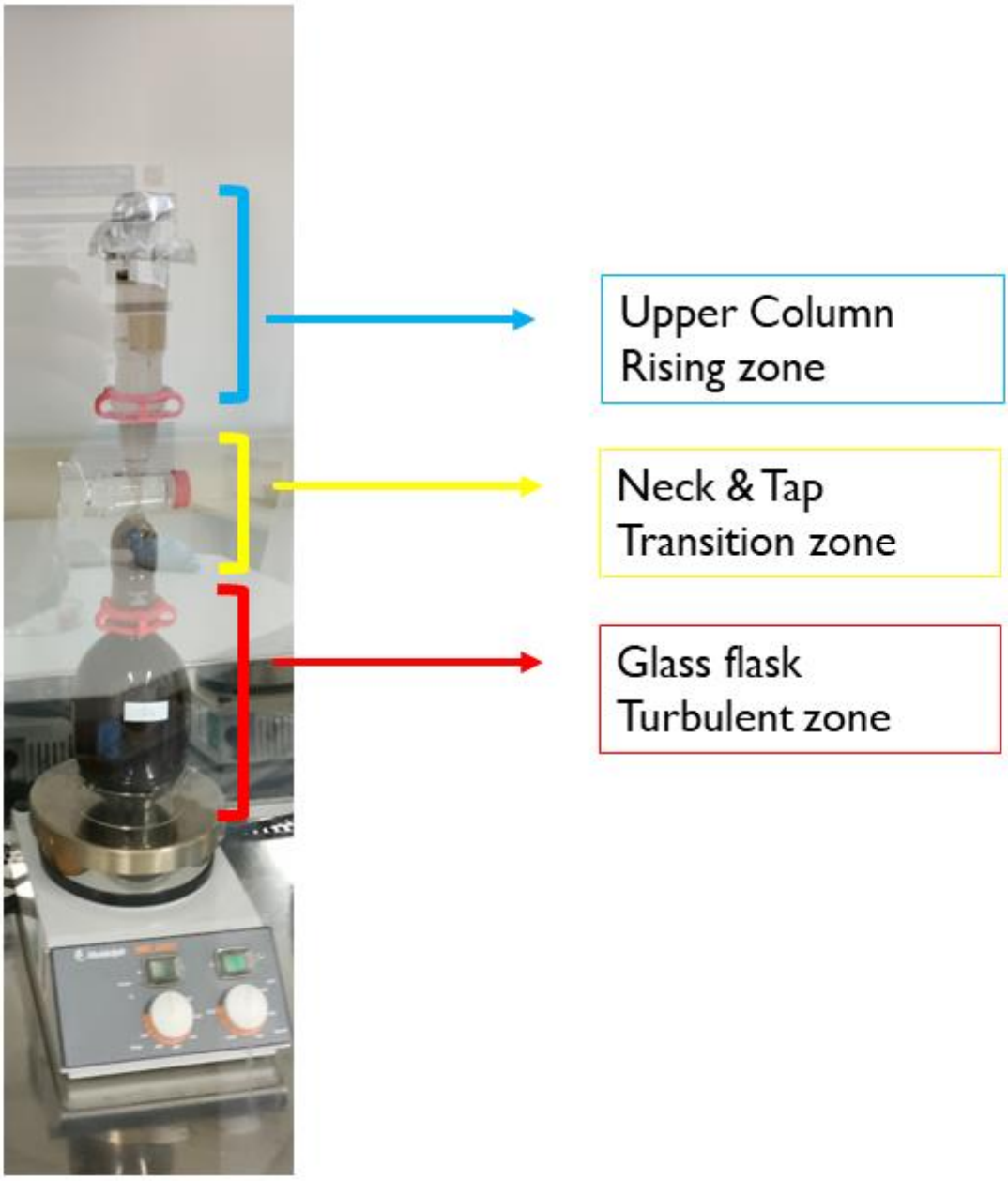

Figure 4 - Image showing setup of first density separation flask and density separator

Step 2 – Microwave assisted hypochlorite digestion

After density separation, I poured the residual at the top column from Step 1 (Figure 4) into the filtration unit without rinsing with any other reagents, and vacuum filtered over a rinsed 5 µm PTFE filter membrane. The top of the column is also flushed into the filtration unit using Ethanol (96% and then 30%) plus MilliQ water. The residual was still rich in organic material, and some traces of $ZnCl_2$ remained. To remove any traces of $ZnCl_2$, I then flushed Hydrochloric acid (1.2%) over the membrane.

The loaded filter membrane was then moved into an 80 mL quartz reaction vessel with tweezers, and I added 25 mL Sodium Hypochlorite (NaClO, 10% solution) using a glass pipette alongside a 9mm PTFE stirring rod. NaClO breaks down the organic components in the sample so that they can be removed in the following flushing steps. The vial was then capped with a rinsed filter to prevent ingress of material, and a ActiVent cap to seal the reaction vessel.

The vials were loaded into a microwave assisted digester (Discover SP-D 80 with Explorer autoloader, CEM Inc.) and I set it to 45 degC for 24h, stirring activated. The temperature of 45 degC was used as the setpoint to prevent melting of polymers; average temperature across multiple cycle runs was 47 degC.

Step 3 – Cellulase

After the cycle completed the vials were removed from the microwave assisted digester. A rinsed filtration unit with a 5 µm filter as used in Step 1 was prepared for each sample. I flushed the contents of the quartz vial onto the filter membrane and rinsed with MilliQ water. The conical flask under the filtration unit **must** be emptied after the MillIQ flush and before further rinsing is undertaken to prevent the formation of chloroform ($CHCl_3$) in the presence of ethanol and sodium hypochlorite (NaClO).

The vial and filtration unit are rinsed with 96% and 30% Ethanol, and MilliQ water to result in a loaded filter membrane as shown in Figure 5. After the vial appeared visually clean, I then filled it with MilliQ and sonicated for 10 seconds in a water bath to release any particles that had clung to the sides of the digestion vial.

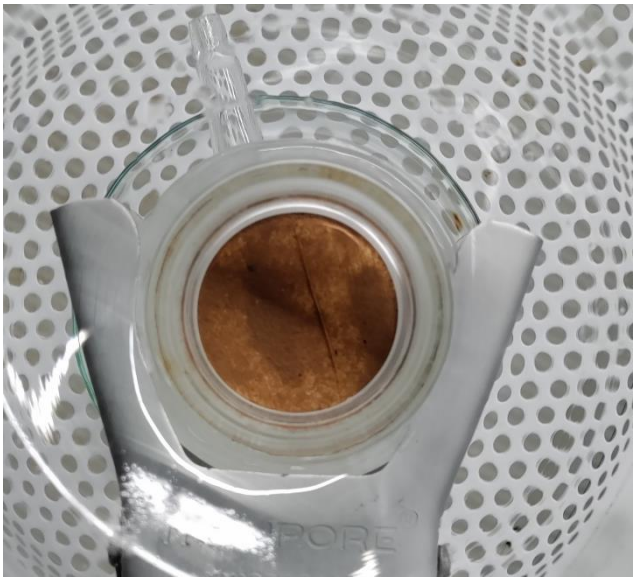

Figure 5 – PTFE filter membrane after microwave digestion with microplastics, residual organics and lithogenics

The residual material (Figure 5) still contains more resistant organic material and cellulosic components (e.g., wood and plant fragments), and as such further processing introduced an enzyme to break down such cellulosic material (Cellulase TXL, ASA Spezialenzyme GmbH).

3 mL TXL Cellulase was buffered with 12mL buffer solution (CH3COOH + CH3COONa, 1 mol L^{-1} , pH = 5) and I added this on top of the membrane. The entire filtration unit was then capped with aluminium foil and a plastic-free elastic band to seal the top, with a petri-

dish lid placed underneath each filter stem to prevent spillage (Figure 6), and this was then incubated at 40 degC for 24 hours in an incubation chamber.

I regularly checked samples to see if the solution ran through the filter, if so it proceeded directly to the next step.

Figure 6 - Example of sealed filtration unit

Step 4 – Second Sodium Hypochlorite

This is an addition to the Helmholtz-Zentrum Hereon's protocol; I added a step of an additional sodium hypochlorite stage following noticeable growth of fungi on the slides, presumed due to the exposure of the dry filter membrane during incubation. Adding this

additional step helped improve imaging times and aided slide preservation by removing as much microbial spore content as possible from the sample.

I removed the filter unit from the incubator (Step 3), rinsed with 96% and 30% ethanol and MilliQ, and 25mL NaClO (10%) was added via glass pipette, then resealed with aluminium foil and plastic-free elastic bands, and left to sit on the membrane for 24 hours or until it ran through. A petri dish lid was left under each filter stem to capture any run-through (Figure 6).

Step 5 – First Hydrogen Peroxide

To break down any residual organic material, it is necessary to further purify the sample with hydrogen peroxide. Removal of organic material further enhanced the imaging process.

15 mL of Hydrogen Peroxide (H_2O_2, 30%) was added to the membrane via glass pipette and capped with aluminium foil and plastic-free bands, and left to sit on the membrane for 24h, or until it ran through. A petri dish lid was again left under each filter stem to capture any run-through (Figure 6).

Step 6 – Second Density Separation

After the peroxide rinse, the filter contained a refined portion of particles, however biofouling and organic aggregations has previously resulted in particles with densities > 1.7 g cm^{-3} persisting the initial density suspension. To this end, I repeated the density separation but with a smaller volume of the $ZnCl_2$ solution and in a separation funnel.

The filtration unit and membrane were rinsed with Ethanol (96% and 30%) and MilliQ water, and then I held the filter membrane over a separator funnel via an analytical funnel. Using a Nalgene (FEP) reagent bottle, Zinc Chloride (approx. 25 mL) was used to release the particles from the filter membrane, and then the filter paper was discarded, and the funnel was rinsed with ZnCl2, ensuring that the tip of the funnel did not make contact with the surface level of the suspension to prevent loss of particles.

The flask was then capped with a ground glass stopper, shaken vigorously for 20 seconds, and then I withdrew the stopper whilst simultaneously rinsing with Zinc Chloride until it was filled to the 50 mL mark on the vessel.

The separatory funnel was left without stirring to settle for a further 24h (Figure 7). After this time, I drained the lower 25mL (50%) via the tap to remove the heavier particles. The remaining fraction (approx. 25 mL) then proceeded to Step 7.

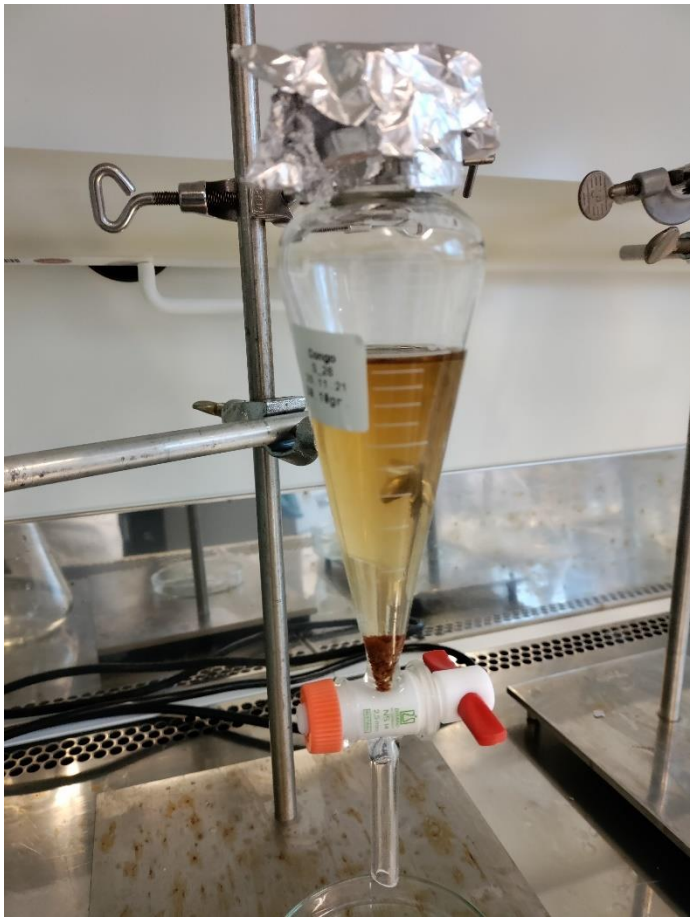

Figure 7 - Second density separation after 24h settling showing settling of denser particles and floating of lighter particles

Step 7 – Second Hydrogen Peroxide

As I identified in Step 6, the result of removing the layers of biofouling resulted in the liberation of organic material that had otherwise not been affected by the previous processes. As such I defined an additional peroxide rinse in the protocol.

The upper fraction from the separatory funnel was then first emptied into a filtration unit with a 5 µm PTFE filter.

The separatory funnel and filtration unit were to be rinsed thoroughly with an additional step of 1.2% Hydrochloric Acid to remove remaining residues of Zinc Chloride, and then the entire filtration unit should be rinsed with 96% and 30% Ethanol, then MilliQ Water.

Using a glass pipette I applied 25 mL H_2O_2 to the membrane, and the same capping process (Figure 6) - aluminium foil and plastic-free rubber bands on the top, and petri dishes on the bottom – was applied, the unit was placed in the incubator at 40 degC for 24h or until the solution ran through.

Step 8 – Transfer to Slide

Prior to removing the filtration unit from the incubator, I identified that it was beneficial to prepare the slides and storage media. For each sample, I flushed three Kevley MirrIR (silver coated) slides using 96% and 30% Ethanol, and MilliQ Water, and laid in a 6 cm petri dish in the clean bench. After the slide had evaporated, it was flushed with Nitrogen gas via a fine nozzle, and then using a permanent marker (e.g., Sharpie) I obscured the longest sides of the slide to prevent the ingress of light incident to the plane of measurement in the LDIR. This aided with the quality of matches and the repeatability of spectral analyses.

The filtration unit was then removed from the incubator and the filter membrane was detached from the stem. A sterilised container (preferentially a 9cm petri dish) was selected and weighed on a mass balance with lid. I then held the filter with tweezers above the sterilised container and the residue on the filter was released with 5-10 mL EthOH (50%). The lid was then returned in place and the petri dish was weighed to define mass of suspension.

For each slide, I drew 0.5 mL of solution from the petri dish into a glass pipette. Setting a white piece of paper under the petri dish aided in discerning particles for pipetting. I then released the material in the pipette onto the slide in a set manner, as shown in Figure 8 whereby beginning from the lower edge of the slide, a drop is released in a zig-zag pattern whilst ensuring that the liquid did not flow over the edge of the slide. The 9cm petri dish was then weighed after each withdrawal to evaluate the load of the suspension per slide.

A visual overview of the slide laying process is given in Figure 8 and Figure 9.

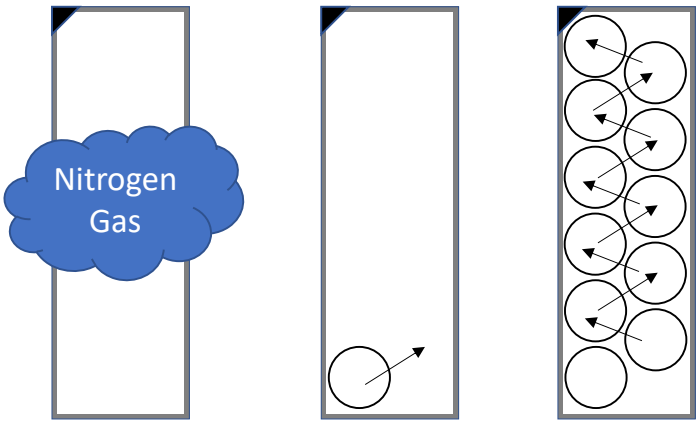

Figure 8 - Slide laying process showing 1mm border (blue) and ground glass corner (black)

I then left in the petri dishes in the clean bench, with the lid being left at a slight angle to aid evaporation whilst minimising the risk of airborne contamination. These were then supervised until the ethanol had completely evaporated, at which point the lid was closed and the petri dishes were banded and stored in LDPE bags with silica desiccant pouches to reduce microbial growth.

Once evaporated, all media was then subjected to two hours in a clean bench with a UV-C source to retard microbial growth. I removed borosilicate glass lids during exposure in the clean bench to maximise transmission of UV-C.

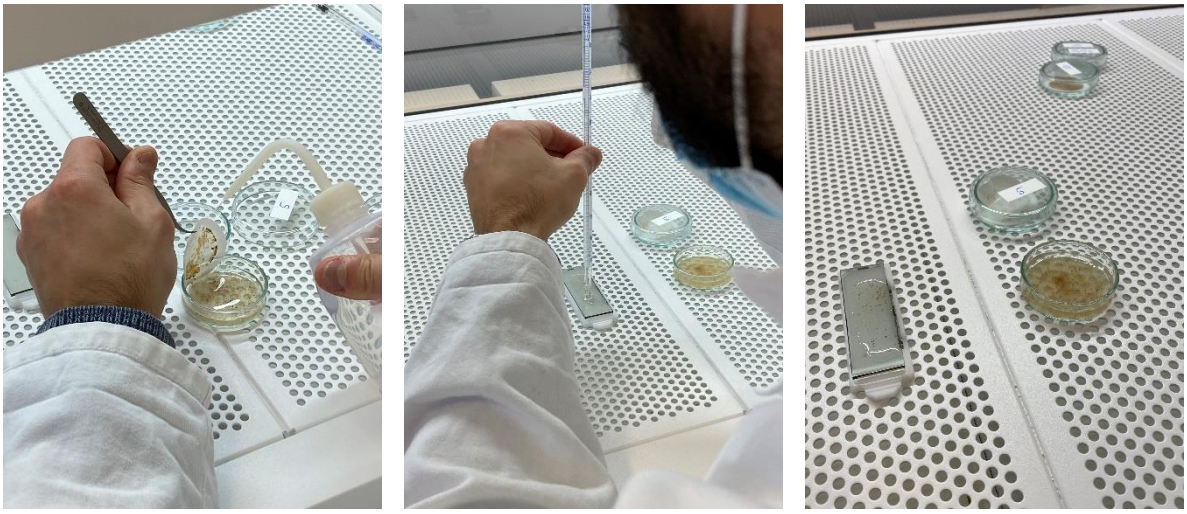

Figure 9 - Slide laying process - Left: Releasing sample from membrane, Centre: Laying of slide, Right: End result, slide in carrier (not yet fully evaporated)

Step 9 - Imaging

Once the samples were transferred onto slides, I undertook imaging of each of the three replicates using the LDIR. I first ran an automated analysis at a minimum size of 10 µm using the local spectral library (Microplastic Starter 1.0) which has been supplemented by the lab with known material from other analyses. The automated analysis identified particles by scanning at 1799 nm and then performed a single analysis within the particle boundary and compares this to the spectral library (Figure 10). The outer 1 mm of the periphery of each slide (Figure 8) was excluded from the analysis to avoid analysing possible contamination from the operatory or during storage.

After the automated analysis completed, any potential microplastic particles with a match quality less than 80% (0.8) were rejected, and I then re-evaluated the particles by reviewing each class of particle and performing subsequent spot analyses and line analyses at different areas within the particle boundary, as the original spot analysis performed by the system (shown in Figure 10) was sometimes on a thicker or thinner part of the particle and therefore affected the measured spectral response. I reviewed different areas to attempt to confirm the classification, as the spectral acquisition can be affected by varying thickness, biological overgrowth, particle aggregation, and weathering. Images were exported of clearly defined particles to aid further analysis.

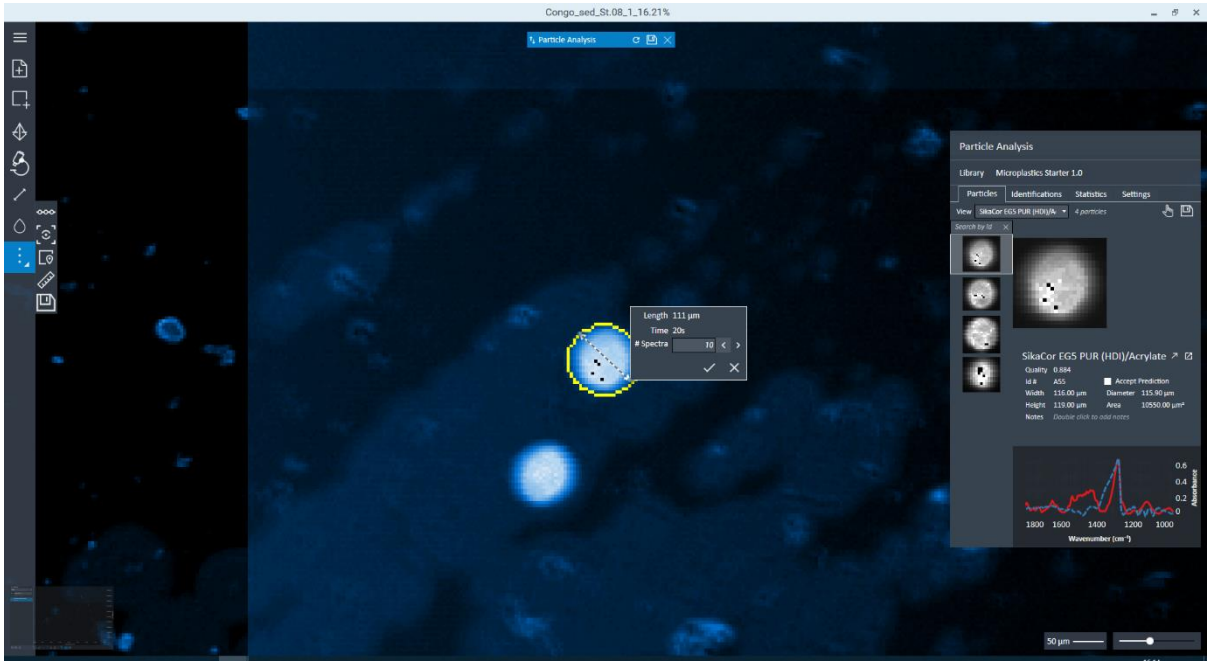

Figure 10 - Screenshot of Agilent Clarity particle analysis software showing identification of particle boundaries

Particle analysis limitations

The LDIR apparatus offered many benefits over standard spectroscopy techniques (i.e., Raman, FTIR) and these are directly associated with the automated, high-resolution particle analysis being possible with the LDIR, against manual spot analyses with Raman spectroscopy. Raman spectroscopy is well-developed spectral imaging technology and has a minimum size limit of 1 µm, but is time consuming and has a limited resolution for imaging. (Luo *et al.* 2022)

LDIR counters this through fast imaging times and the specific apparatus in use at the Hereon provides combination LDIR, ATR crystal, and high power visible light microscopy. However, the spectral field in which the LDIR is able to analyse particles (wavelength 975-1799 cm^{-1}) results in a confining of the usability of this software (Araujo *et al.* 2018; Luo *et al.* 2022). Ultimately, Luo et al. decided that this means plastics below 10 µm are not measurable due mostly to the limitations of the particle detection process alone, and not the capabilities of the spectral analysis, and this is reflected in the lab work protocol employed, however the high percentage of discarded particles in my lab work indicated that even at around the 10 µm border the certainty of the identifications is poor, and this was confirmed by Luo et. al. according the work of Scircle *et al.* (2020) and Samandra *et al.* (2022) who previously set their limit at 18 µm.

I identified a number of polymers, especially Polyethylene Chlorinated and Acrylates which have defining spectral peaks outside of the imaging range of the LDIR, and therefore matrix particles or organic material were often be mis-identified as PE-Cl within wavenumbers 975-1799 cm^{-1}. This created a windowing effect (Figure 3) where my understanding of a particle was clipped by the range of the LDIR apparatus, and therefore these particles that fell out of the automated analysis would have been critical in building a complete understanding of the makeup of all particles in a slide, however, were simply discarded.

Therefore, in this thesis I cautiously excluded any particles that fall within this query group (PE-Cl, Rubber, Acrylates, Polyacetal) where the hit rate was <0.9. It would be possible to manually analyse each queried particle with the ATR crystal to obtain specific results, however the quantity of particles on the slides and the destructive process of the ATR crystal resulted in this not being undertaken.

I am also further limited by the comparison of these results from the LDIR with the other libraries available due to the influence of results on spot vs. whole sample analysis, as identified by (Primpke *et al.* 2020). Due to the difference in analysis methods, with spot spectral analysis from the LDIR gaining different results to whole sample pyrolysis.

Grain sizing

I analysed the grain size distribution of each sample prior to microplastic separation using a laser particle sizing apparatus (Analysette 22 MicroTec plus by Fritsch GmbH, Idar-Oberstein, Germany).

Separate samples were already taken from the freeze-dried cores. I homogenised each sample by hand with a metal scoop prior to dispersal in the sampler unit to rectify any settling or sorting during storage.

Data evaluation

After imaging and re-evaluation, I exported a spreadsheet of all the particle characteristics. A customised grouping and classification spreadsheet was provided by the centre which took the raw data from the machine and grouped it by polymer type/family, as the library does not allow for grouping, and then binned the data by size classes. The output of this is presented in Table 3.

I found that the particle grouping spreadsheet provided by the Helmholtz-Zentrum Hereon was limited in functionality due to the restriction on column position and grouping types. To mitigate this, and also aid in replicability of the data analysis, I began a second package of work to develop a data analysis workflow in R. This is covered in a supplementary report; however, the code package is publicly available[2] and the code package has been used to create the grouped output used in my report. The raw data of all LDIR measurements can be found in the supplementary materials of this thesis.

[2] https://www.github.com/UtrechtUniversity/reclarify

Extrapolation

The subsampling process I used to lay each slide does not provide for a true aliquot of the sample as we have a preferential operator bias for larger/easily visible particles in solution (Nel *et al.* 2019), as well as the residence of particles in the pipette after laying (López-Rosales *et al.* 2022).

As such I calculated only the minimum microplastic load from each slide using the following equation, which can be used for total plastic load as well as for each polymer. This was decided as Karlsson *et al.* (2020) identified that distribution of microplastic particles within slides follows a Poisson distribution, i.e. the presence of each particle is independent of the presence of other particles in the sample.

My extrapolation equation assumed that all of the particles present in the sample have been detected in the slides measured, as following the logic of Karlsson *et al.* (2020) there would be no reliable way to predict average or maximum microplastic concentration in a sample that follows a Poisson distribution. All of the particles were summed, corrected for the percentage of the slide imaged (where this was not 100%) and then extrapolated per kilogram of sediment:

$$load_{kg} = \left[\sum_{i=1}^{n}\left(load_i \times \frac{1}{\%_i}\right)\right] \div w_{sed}$$

where:

$load_{kg} = Microplastic\ particle\ load\ per\ kilogram\ sediment\ \left[\frac{n}{Kg}\right]$

$load_i = Particles\ detected\ per\ slide\ [n]$

$\%_i = Proportion\ of\ slide\ imaged$

$w_{sed} = Weight\ sediment\ at\ 1st\ Density\ Separation\ for\ all\ slides\ in\ sum\ [Kg]$

In order to produce replicable results, it was necessary to choose a consistent set of plastics for extrapolation, as a number of plastic classes in the LDIR were subject to poor hit quality rate. I defined the following list of plastics with good repeatability following testing.

Plastics with unique spectra outside the detection window of the LDIR (Figure 3) were discarded due to their high potential for misidentification.

Natural particles were considered to be any silicate or organic material detected by the LDIR, as well as any material which correlated to the natural material (matrix) defined in the

library provided by the Helmholtz-Zentrum Hereon. Furthermore, the spectra correlating to the PVC Liner used in the transportation of the cores was excluded from the spectra matching routine. The resulting extrapolated values are given in Table 4 and may be considered the minimum microplastic load in the system.

Procedural blanks

I ran four procedural blanks whereby I exposed empty processing units to the same reagents and processes as sediment samples, however no sediment was added to the system. This was to act as a control against and monitoring of microplastic contamination from the process or from me as operator.

No blanks showed plastic contamination.

Contamination protocol

Due to the omnipresence of plastic products in our living and working environments, it is unfortunately not possible to rid the laboratory of everything plastic based. Stringent protocols were installed at the lab, with enforcing of natural fibre clothes and lab coats, and dust filtration and trapping controls in place.

All glassware was rinsed thoroughly following the protocol (see General working procedure, p. 23) and where possible all lab work was completed in a laminar flow bench to minimise airborne contamination. Air filters were permanently engaged in the microplastic analysis lab and regular cleaning of floors and surfaces in combination with floor dust traps (sticky pads by entrances) to prevent import or (re)mobilisation of microplastic through dirt/dust.

Despite these efforts being made in the laboratory to minimize this, and our working to the stringent protocol, there were still issues with local contamination. The MirrIR slides were delivered in a white polypropylene box, which left visible contamination on the slides. In response to this, an additional step of rinsing the slides with compressed Nitrogen was introduced, both before the sterilisation (to prevent the melting of particles to the slide) and immediately before slide deposition (to remove any cross-contamination).

Furthermore, PTFE slides were delivered in a plastic carrier made of polycarbonate and another undefined light thin plastic film. I washed filters and equipment to reduce

contamination, and this has been reflected in the contents of the procedural blanks, however, is acknowledged as a possible source of contamination in the process.

Figure 11 - Photograph of polypropylene carrier for microscopy slides

Sample sterilisation and preservation

Wet sediment samples were held in cold storage (0-5 degC) at the Helmholtz-Zentrum Hereon. Freeze-dried sediment samples were stored in the lab at room temperature.

Microbial overgrowth was noticed in some slides, and as such I included an additional sodium hypochlorite step. However, there was inevitable microbial growth even after this step. As such it was necessary to take further efforts to deactivate any remaining microbes.

I identified that for proper sterilisation it was necessary to leave the glass petri dish slightly open during the sterilisation process, as borosilicate glass hinders transmission of UV-C, and so the clean bench was emptied and cleaned down before the sterilisation of the slides took place. After sterilisation all media was stored in a sealed LDPE bag with desiccant packs

Results

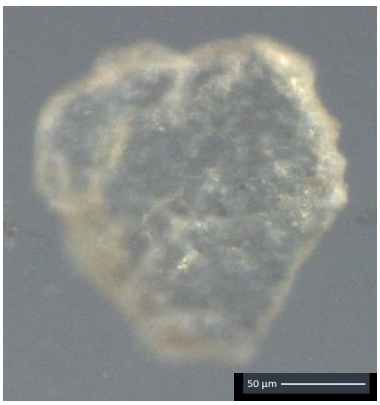

Polyethylene (PE) Particle

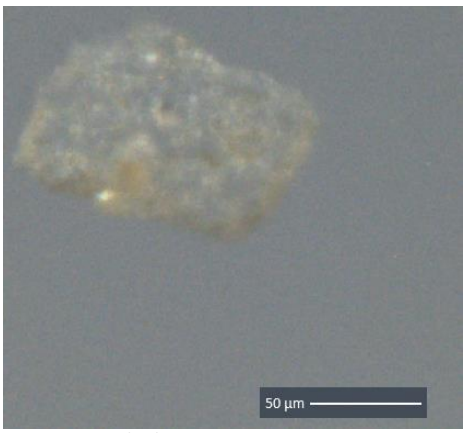

Polyurethane (PU) Particle

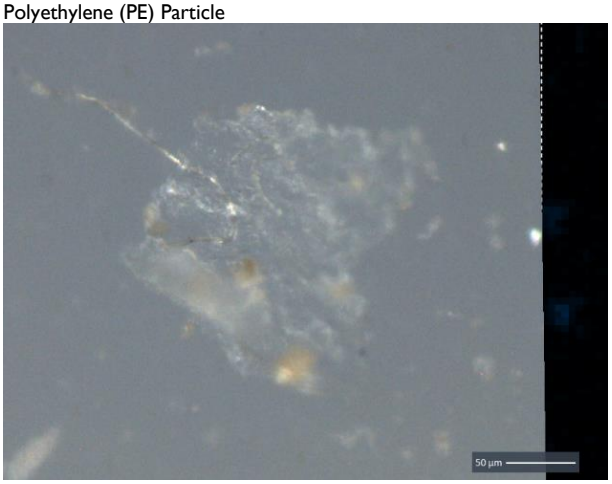

Polytetrafluoroethylene (PTFE) Particle

Polystyrene (PS) Particle

Polypropylene (PP) Microbead

Polypropylene (PP) Fragment

Figure 12 – Example of microplastic particles found during analysis

I found microplastics in all of the samples analysed, an example of particles of various polymer types is shown in Figure 12. Modal polymer types were Polypropylene, Polyurethane, and Polyvinyl Chloride. The results of my laboratory work are presented as a per-slide table (Table 2, p.48), and also as a summary table (Table 3, p.49).

Microplastic load and spatial variation

Microplastic load in the system was highest in the proximal reaches but concentrated also in the distal sections. Microplastic load ranged from 566 to 9138 microplastics per Kg sediment. The out of canyon section contained the lowest microplastic concentration (831 MPs Kg^{-1}) however there was only one sample analysed. Cores within the canyon contain between 2 and 10 times more microplastics per kilogram sediment when compared to the core taken from outside the canyon (Sample S_22).

The lobe had the highest average concentration (mean 6719 MPs Kg^{-1}, n=2) however the variation between the two samples was approximately 5000 particles. This is displayed graphically below, and it is of note that the Terrace (mean 2607 MPs Kg^{-1}, n = 6) and Thalweg (mean 1997 MPs Kg^{-1}, n = 6) provided the majority of the microplastics analysed despite their averages being lower (Figure 13).

Additionally, there appears to be a concentration of microplastics at the near-shore cores, however far-offshore cores still present high loads of microplastics (Figure 14).

This data has been further presented graphically as in the maps given on the A3 insert showing the distribution of microplastics per kilogram along the Congo Canyon System (Figure 19) which can be read in conjunction with the locations of the cross sections (Figure 14).

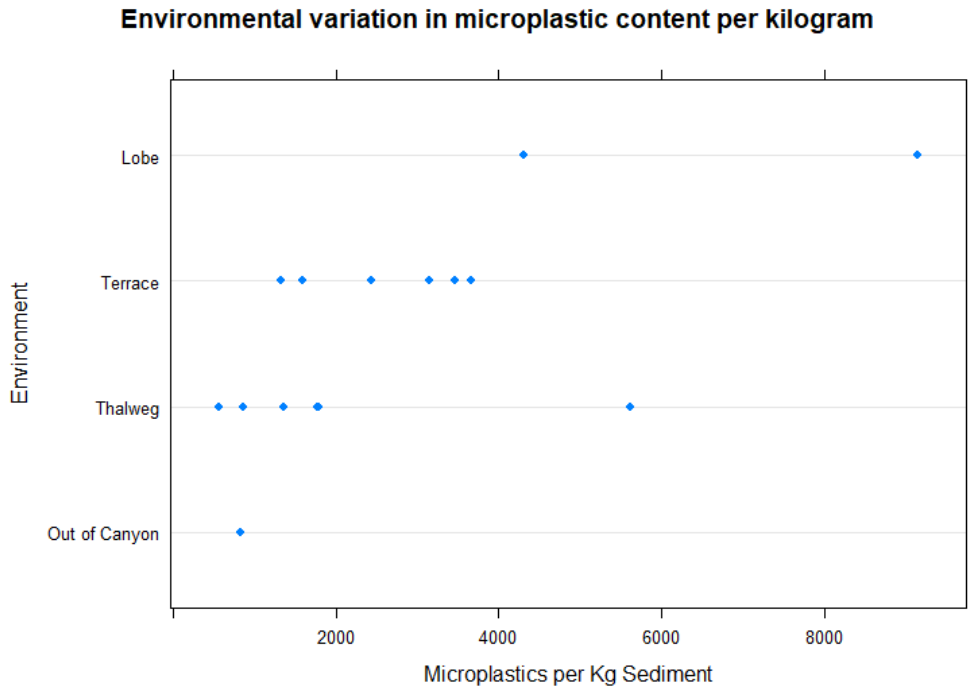

Figure 13 - Comparison of microplastic load per kilogram sediment against depositional environment showing increase in lobe and terraces compared to channel and thalweg

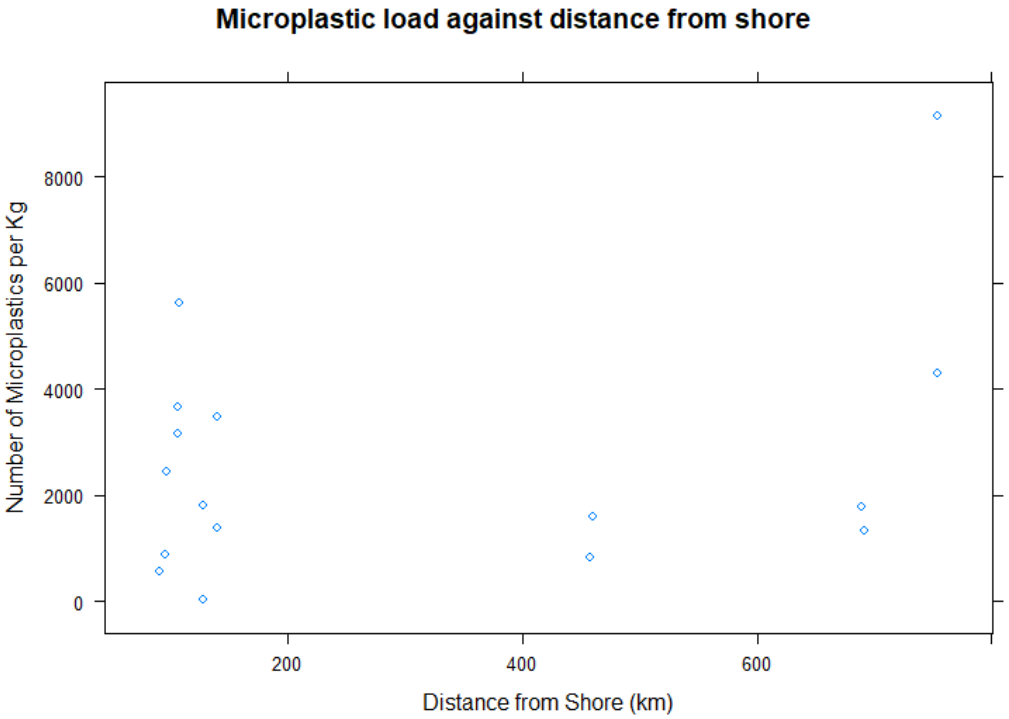

Figure 14 - Graph showing variation in microplastic concentration per kilogram when compared to straight line shore distance, proximal and distal deposits having the highest microplastic content per kilogram

Comparison of grain size to microplastic load

Microplastics were present in all samples and as such there is a baseline level of microplastic content that is present throughout the canyon (Figure 15, Figure 16, Figure 17, and Figure 18 - overleaf). Two of the coarsest samples (D_{50} >50 µm) contained a high microplastic load, however there were only 3 samples with a coarse (sandy) D_{50} measured. The sample located outside of the canyon (Figure 15, red marker) contained one of the lowest concentrations of microplastics (831 particles Kg^{-1}).

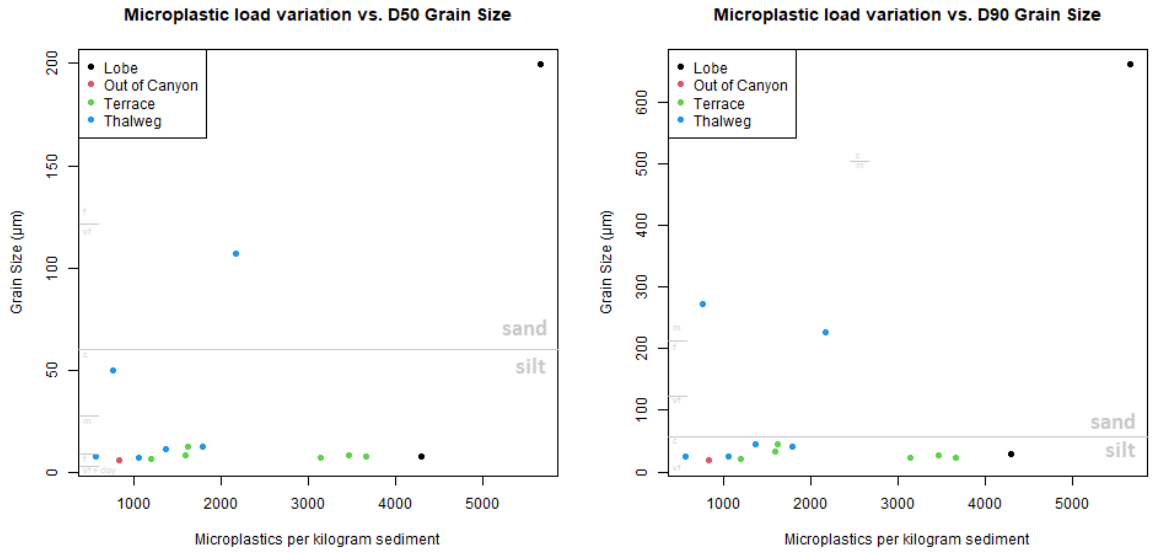

Figure 15 - Microplastic load against mean (D50) and coarse (D90) sediment grain size, lobe sample >600 µm D90 indicates high presence of woody organics in sample

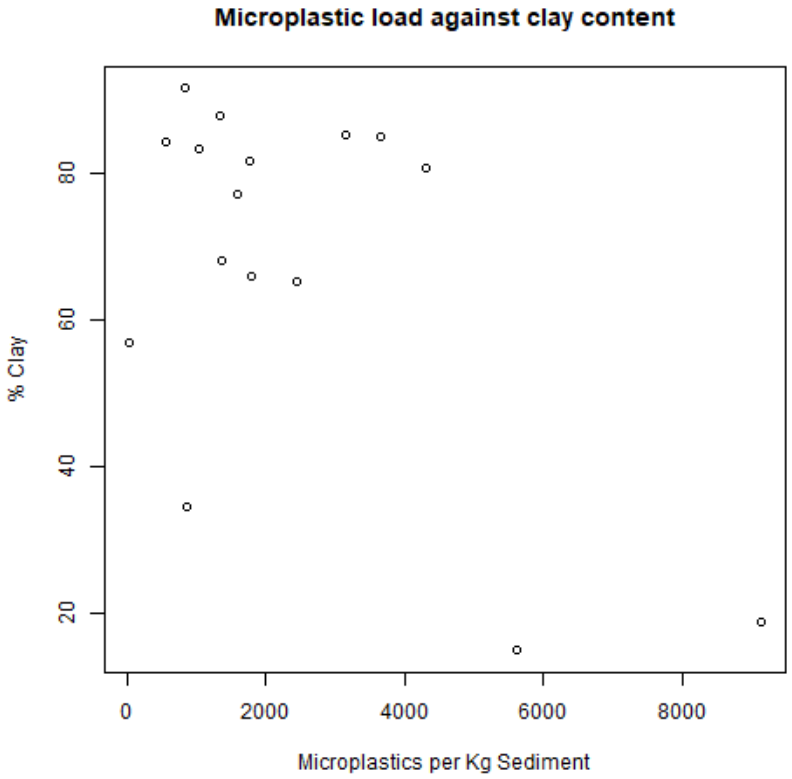

Figure 16 - Microplastic load against clay content

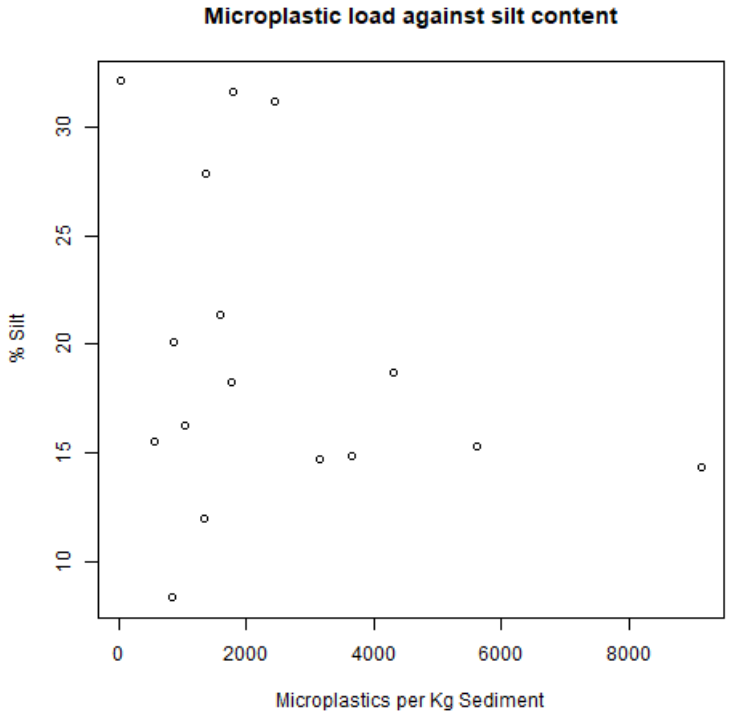

Figure 17 - Microplastic load against silt content

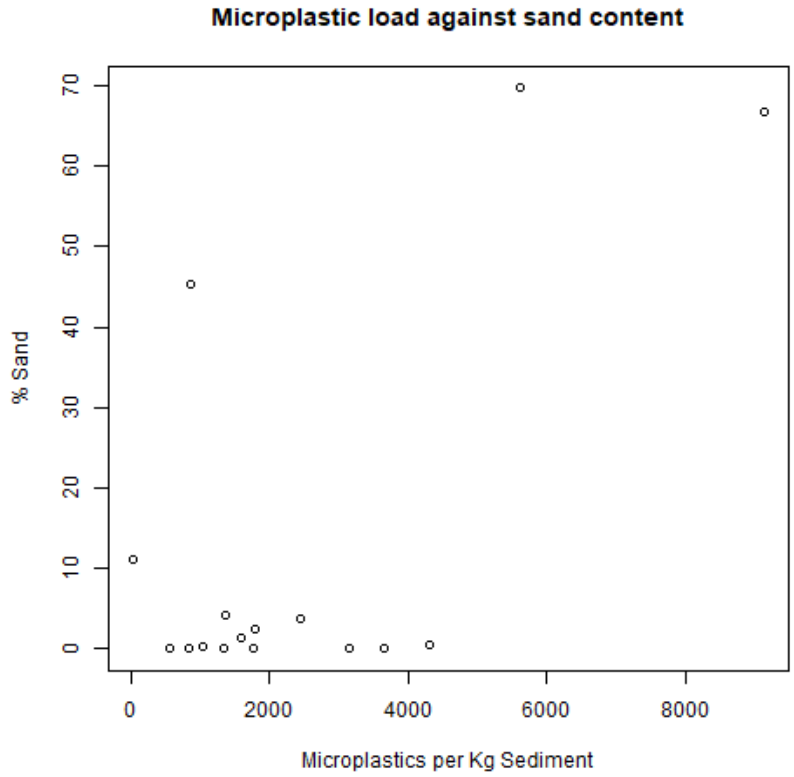

Figure 18 - Microplastic load against sand content

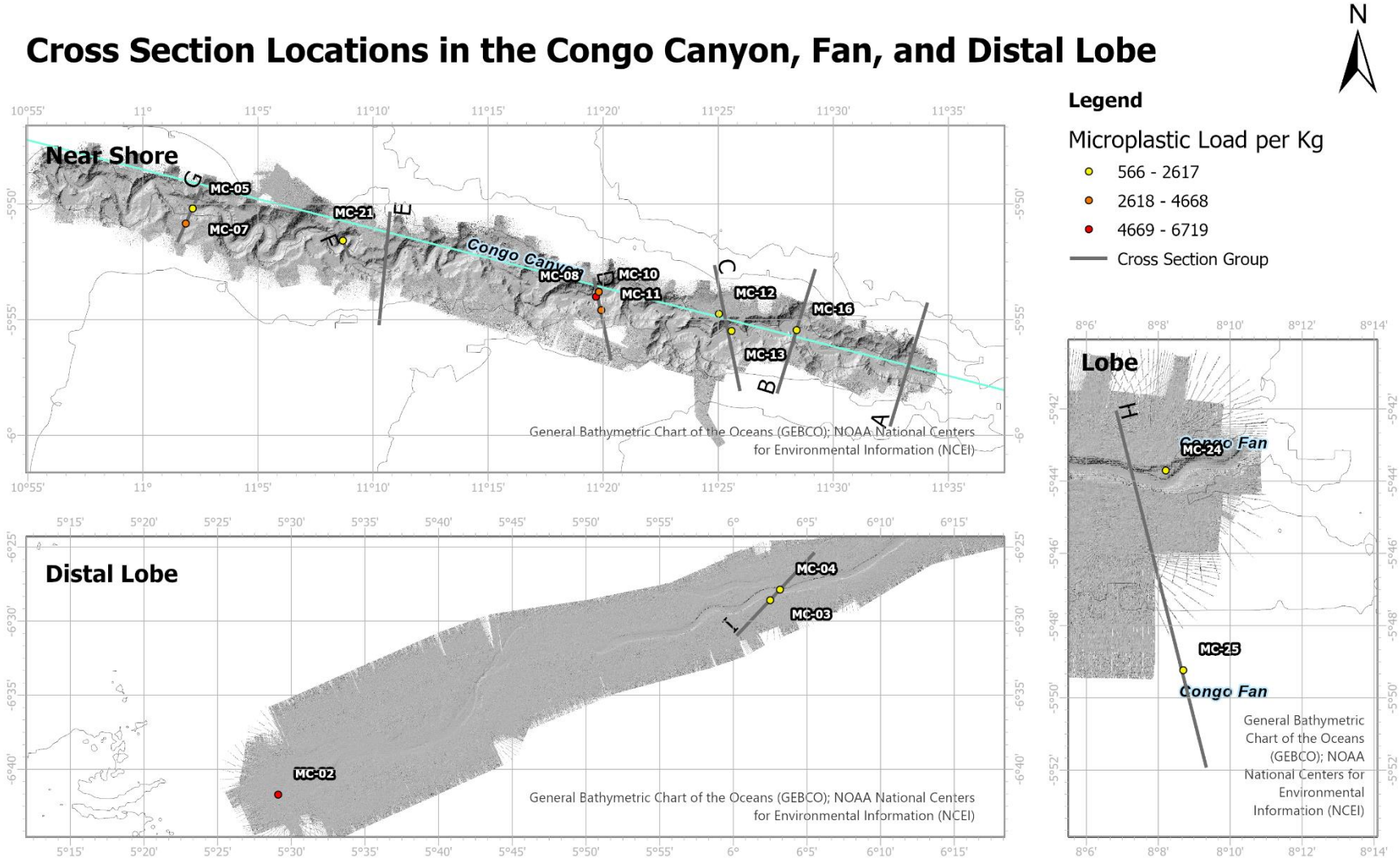

Figure 19 – Approximate cross section locations in the Congo Canyon Systems showing channel profile, including microplastic distribution per kilogram sediment

Table 2 – Slide data

Sample	Slide number	Depositional environment	Weight sample [g]	Slide suspension [g]	Sample D_{50} [µm]	% Slide Imaged	Polyamide (PA)	Polycarbonate (PC)	Polyethylene (PE)	Polyethylene Terephthalate (PET)	Poly(methyl methacrylate) (PMMA)	Polypropylene (PP)	Polystyrene (PS)	Poly tetrafluoro-ethylene (PTFE)	Polyurethane (PU)	Polyvinyl-chloride (PVC)	Natural Particles [-]	Imaged MPs [-]	Discarded Particles [-]	Total Slide Particle Load [-]
S_04	01	Thalweg	30.79	0.49	106.87	100%	0	1	14	1	0	0	1	1	0	14	294	32	1970	2296
	02			0.85		100%	0	0	3	4	0	0	0	11	6	11	314	35	1840	2189
	03					100%	0	3	0	6	0	1	0	81	1	14	1269	106	5409	6784
S_07	01	Lobe	30.75	1.05	199.40	100%	0	0	13	7	0	62	0	0	0	8	837	90	2160	3087
	02			0.68		100%	0	0	8	1	0	32	0	0	37	6	658	84	1132	1874
	03					100%	0	0	0	2	0	27	0	0	72	6	3842	107	5996	9945
S_08	01	Lobe	30.00	1.02	8.05	100%	0	0	6	0	1	14	0	0	2	0	352	23	1612	1987
	02			1.03		33%	0	0	0	0	0	8	0	0	1	2	57	11	371	439
	03			1.06		100%	1	0	2	1	0	13	0	0	0	56	869	73	769	1711
S_11	01	Thalweg	30.00	0.76	11.49	100%	0	0	0	0	0	3	1	0	0	0	296	4	1122	1422
	02			0.97		100%	0	0	6	0	0	0	4	0	1	0	561	11	3382	3954
	03			0.98		50%	0	0	0	1	0	0	0	0	1	11	166	13	1105	1284
S_15	01	Terrace	30.01	1.29	8.82	**Slides 01 & 02 not imaged due to fungal overgrowth**														
	02			1.49																
	03			0.99		25%	0	0	0	1	0	5	1	0	0	19	422	26	2436	2884
S_16	01	Thalweg	30.09	0.63	50.00	100%	0	0	0	3	0	1	0	0	3	5	432	12	950	1394
	02			0.59		100%	0	0	0	0	0	0	0	0	2	1	246	3	1024	1273
	03			0.51		100%	0	0	0	8	0	2	0	0	1	0	520	11	1115	1646
S_19	01	Terrace	30.17	0.96	8.82	25%	0	0	5	0	0	0	4	0	1	2	564	48	File corrupted[3]	
	02			1.06		**Slides 02 & 03 not imaged due to fungal overgrowth**														
	03			0.94																
S_22	01	Out of Canyon	30.08	0.40	6.12	100%	0	0	1	1	0	0	2	0	0	1	117	5	584	706
	02			0.48		100%	0	0	0	0	0	3	3	0	1	6	296	13	1285	1594
	03			0.68		100%	0	0	0	0	0	1	1	0	0	5	301	7	828	1136
S_24	01	Terrace	30.17	0.66	7.65	100%	6	0	2	1	0	2	0	0	0	25	298	36	786	1120
	02			0.40		100%	2	0	5	0	0	9	0	0	4	31	573	51	1665	2289
	03			0.39		100%	0	0	4	0	0	0	0	0	1	3	794	8	1128	1930
S_26	01	Terrace	30.10	0.79	8.09	100%	0	0	1	0	0	3	5	0	0	24	515	33	1488	2036
	02			0.67		75%	0	0	0	2	0	4	3	1	1	38	999	49	948	1996
	03			0.88		100%	0	0	0	0	0	3	1	0	0	8	496	12	583	1091
S_28	01	Terrace	30.72	0.84	44.64	100%	1	0	5	0	0	5	0	1	0	35	843	47	2115	3005
	02			1.08		100%	2	0	1	1	0	4	0	0	2	15	1769	25	1984	3778
	03			0.36		100%	0	0	0	0	1	0	0	0	0	2	593	3	670	1266
S_29	01	Thalweg	30.14	0.54	12.89	100%	0	0	1	1	0	4	0	0	4	3	434	13	1174	1621
	02			0.52		100%	0	0	2	2	0	6	0	0	10	9	372	29	988	1389
	03			0.37		100%	0	0	0	1	0	2	0	0	5	4	445	12	1037	1494
S_31	01	Terrace	30.01	0.75	21.65	100%	0	0	0	1	0	0	0	0	0	22	446	23	1397	1866
	02			0.70		100%	0	0	2	0	0	1	0	0	0	1	279	4	591	874
	03			0.79		100%	2	0	2	1	0	2	1	0	0	5	671	13	1394	2078
S_33	01	Thalweg	30.43	0.66	25.79	100%	0	0	3	0	0	2	0	0	1	5	436	11	1503	1950
	02			1.80		100%	0	0	5	4	0	0	0	0	6	6	354	21	1113	1488
	03					100%	0	0	6	2	0	7	0	1	4	2	1419	22	3850	5291
S_35	01	Thalweg	30.04	0.46	7.74	100%	0	0	0	0	0	0	0	0	0	1	58	1	120	179
	02			0.44		100%	0	0	1	0	0	0	1	0	0	7	219	9	394	622
	03			0.58		100%	1	0	1	0	0	0	1	0	2	2	376	7	739	1122

[3] The LDIR suffered a fatal error after imaging this slide and the raw data was not retained

Table 3 - Summary Table of Results

Grouping	Core ID	Sample ID	Depositional environment	Sample D_{50} [µm]	Sample D_{90} [µm]	Polyamide (PA)	Polycarbonate (PC)	Polyethylene (PE)	Polyethylene Terephthalate (PET)	Poly(methyl methacrylate) (PMMA)	Polypropylene (PP)	Polystyrene (PS)	Poly tetrafluoro-ethylene (PTFE)	Polyurethane (PU)	Polyvinyl-chloride (PVC)	Natural Particles [-]	Imaged MPs [-]	Imaged MPs (corrected for imaging) [-]	Discarded Particles [-]	Total Slide Particle Load [-]	MPs per Kg Sediment [-]
J	MC-02	S_08	Lobe	8	29	1	0	8	1	1	35	0	0	3	58	1278	107	129	2752	4137	4300
J	MC-02	S_07	Lobe	199	662	0	0	21	10	0	121	0	0	109	20	5337	281	281	9288	14906	9138
I	MC-03	S_31	Terrace	7	22	2	0	4	2	0	3	1	0	0	28	1396	40	40	3382	4818	1333
I	MC-04	S_33	Thalweg	8	26	0	0	14	6	0	9	0	1	11	13	2209	54	54	6466	8729	1775
F	MC-05	S_11	Thalweg	11	45	0	0	6	1	0	3	5	0	2	11	1023	28	41	5609	6660	1367
F	MC-07	S_15	Terrace	9	26	0	0	0	1	0	5	1	0	0	19	422	26	104	2436	N/A[4]	3466
D	MC-08	S_04	Thalweg	107	227	0	4	17	11	0	1	1	93	7	39	1877	173	173	9219	11269	5619
D	MC-10	S_24	Terrace	8	24	8	0	11	1	0	11	0	0	5	59	1665	95	95	3579	5339	3149
D	MC-11	S_26	Terrace	8	24	0	0	1	2	0	10	9	1	1	70	2010	94	110	3019	5123	3666
C	MC-12	S_28	Terrace	13	45	3	0	6	1	1	9	0	1	2	52	3205	75	75	4769	8049	2441
C	MC-13	S_16	Thalweg	50	274	0	0	0	11	0	3	0	0	6	6	1198	26	26	3089	4313	864
B	MC-16	S_35	Thalweg	8	25	1	0	2	0	0	0	2	0	2	10	653	17	17	1253	1923	566
G	MC-21	S_29	Thalweg	13	42	0	0	3	4	0	12	0	0	19	16	1251	54	54	3199	4504	1792
H	MC-24	S_19	Terrace	9	33	0	0	5	0	0	0	4	0	1	2	564	12	48	No Data	N/A[4]	1591
H	MC-25	S_22	Out of Canyon	6	19	0	0	1	1	0	4	6	0	1	12	714	25	25	2697	3436	831

[4] Due to the incomplete imaging of these slides, it is not possible to extrapolate total particle load for the samples

Table 4 - Extrapolated polymers per kilogram sediment

Core ID	Sample ID	Depositional environment	Polyamide (PA)	Polycarbonate (PC)	Polyethylene (PE)	Polyethylene Terephthalate (PET)	Poly(methyl methacrylate) (PMMA)	Polypropylene (PP)	Polystyrene (PS)	Poly tetrafluoro-ethylene (PTFE)	Polyurethane (PU)	Polyvinyl-chloride (PVC)
MC-02	S_08	Lobe	33	0	267	33	33	1167	0	0	100	1933
MC-02	S_07	Lobe	0	0	683	325	0	3935	0	0	3545	650
MC-03	S_31	Terrace	67	0	133	67	0	100	33	0	0	933
MC-04	S_33	Thalweg	0	0	460	197	0	296	0	33	361	427
MC-05	S_11	Thalweg	0	0	200	33	0	100	167	0	67	367
MC-07	S_15	Terrace	0	0	0	33	0	167	33	0	0	633
MC-08	S_04	Thalweg	0	130	552	357	0	32	32	3020	227	1267
MC-10	S_24	Terrace	265	0	365	33	0	365	0	0	166	1956
MC-11	S_26	Terrace	0	0	33	66	0	332	299	33	33	2326
MC-12	S_28	Terrace	98	0	195	33	33	293	0	33	65	1693
MC-13	S_16	Thalweg	0	0	0	366	0	100	0	0	199	199
MC-16	S_35	Thalweg	33	0	67	0	0	0	67	0	67	333
MC-21	S_29	Thalweg	0	0	100	133	0	398	0	0	630	531
MC-24	S_19	Terrace	0	0	166	0	0	0	133	0	33	66
MC-25	S_22	Out of Canyon	0	0	33	33	0	133	199	0	33	399

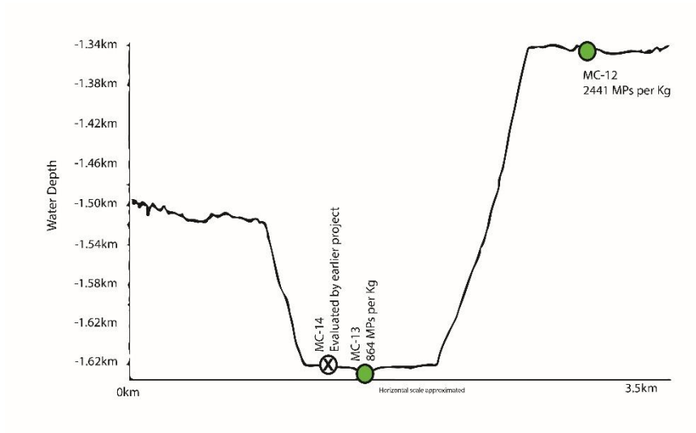

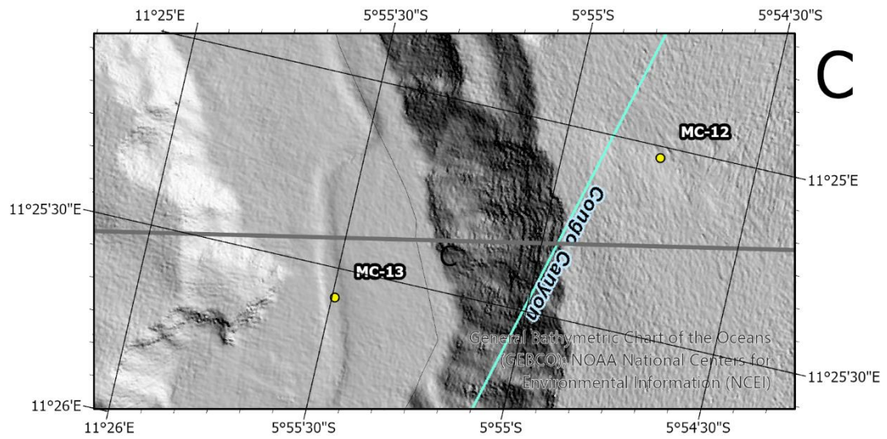

Group C –Most proximal Thalweg transect

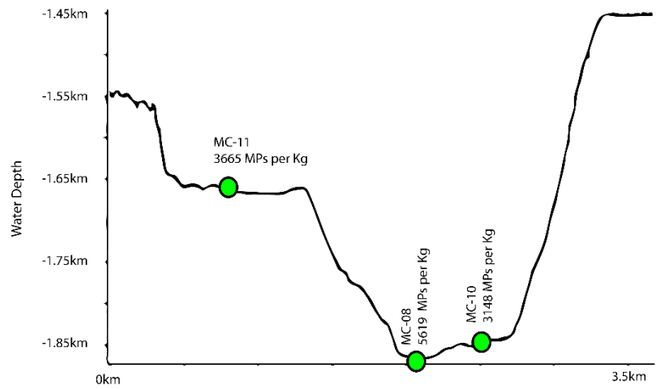

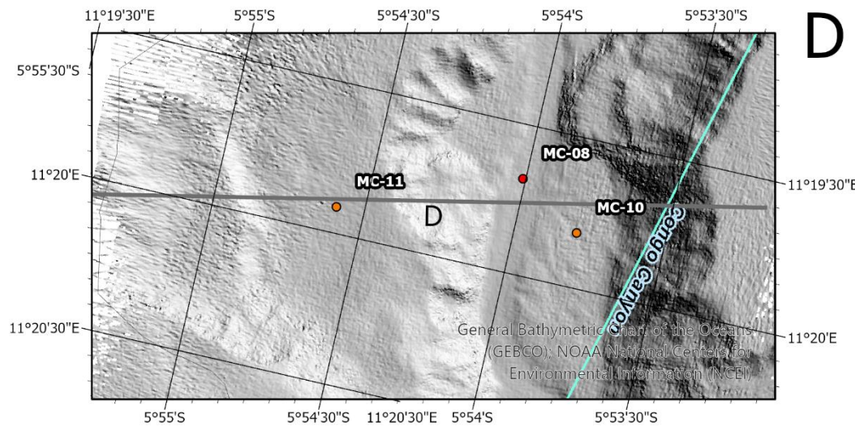

Group D – Proximal Thalweg transect

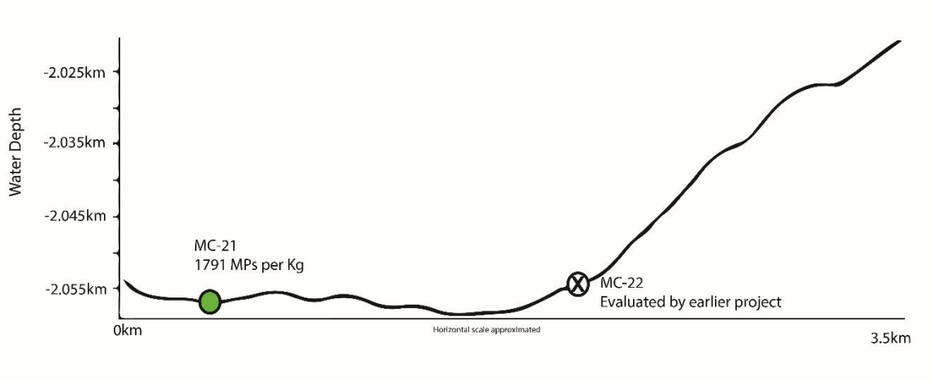

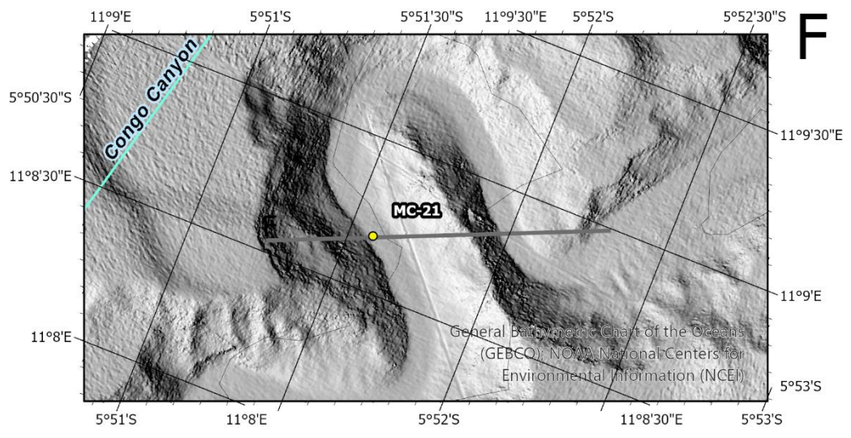

Group F – Meander bend transect

Figure 20 - Cross sectional profiles and birds-eye view of groups C, D, and F showing microplastic load in the canyon, map key conforms to Figure 19

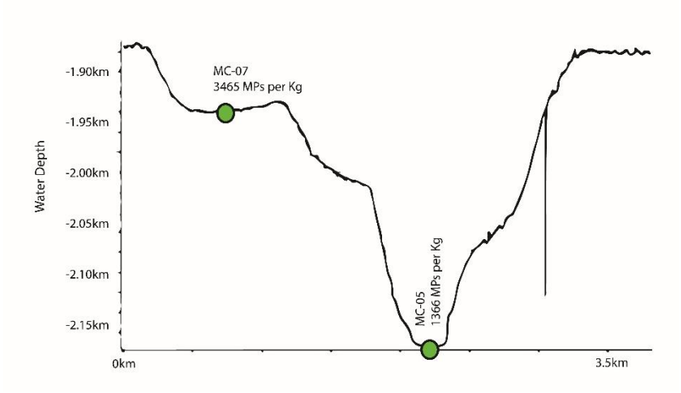

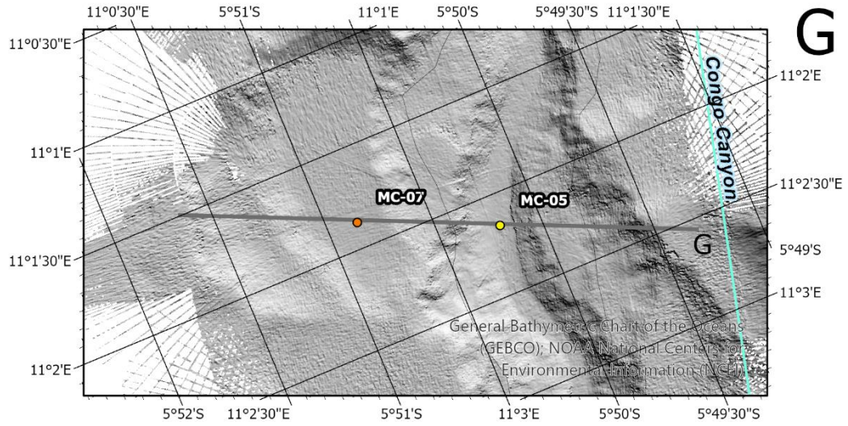

Group G – Distal Mixed Terrace and Thalweg transect (10km downstream MC09-12)

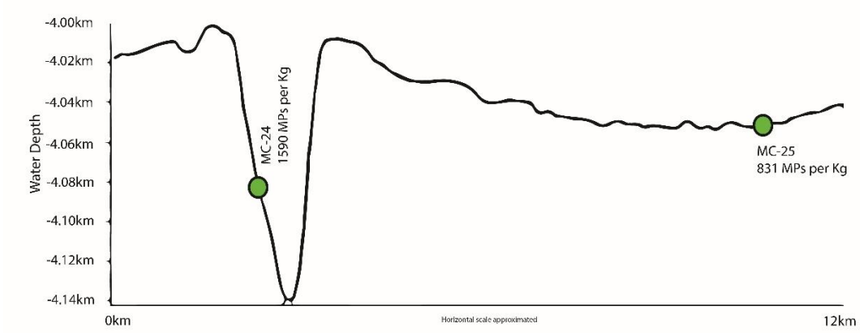

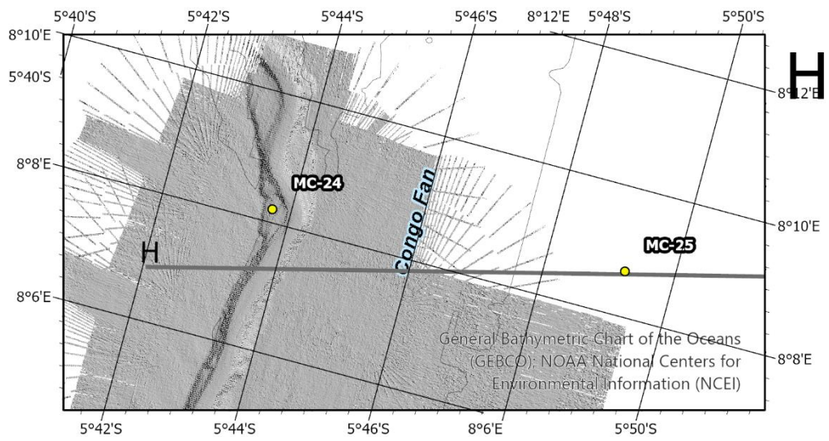

Group H – Very distal submarine channel transect (400km downstream) + Out of Canyon Sample

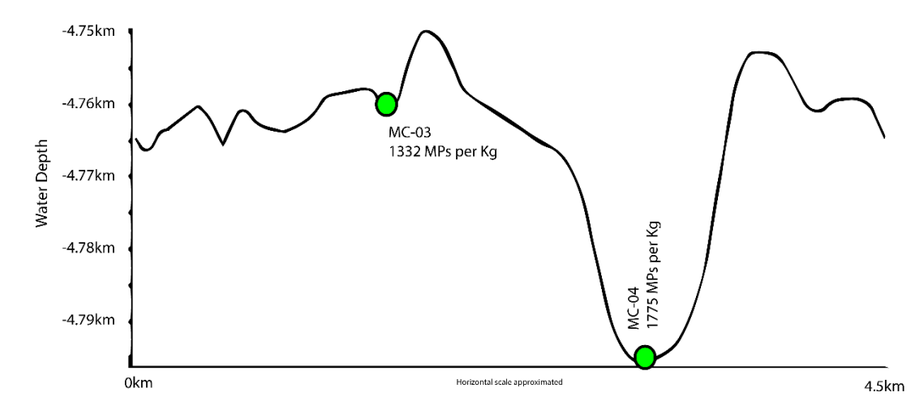

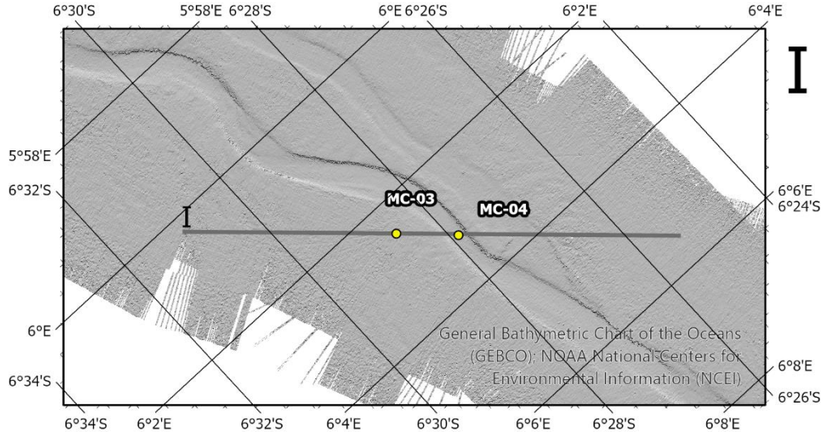

Group I – Most Distal Channel transect (>300km from MC23-25)

Figure 21 - Cross sectional profiles and birds-eye view of groups G, H, and I showing microplastic load in the canyon, map key conforms to Figure 19

Comparison of PP vs PE vs PET Load in the Congo Canyon

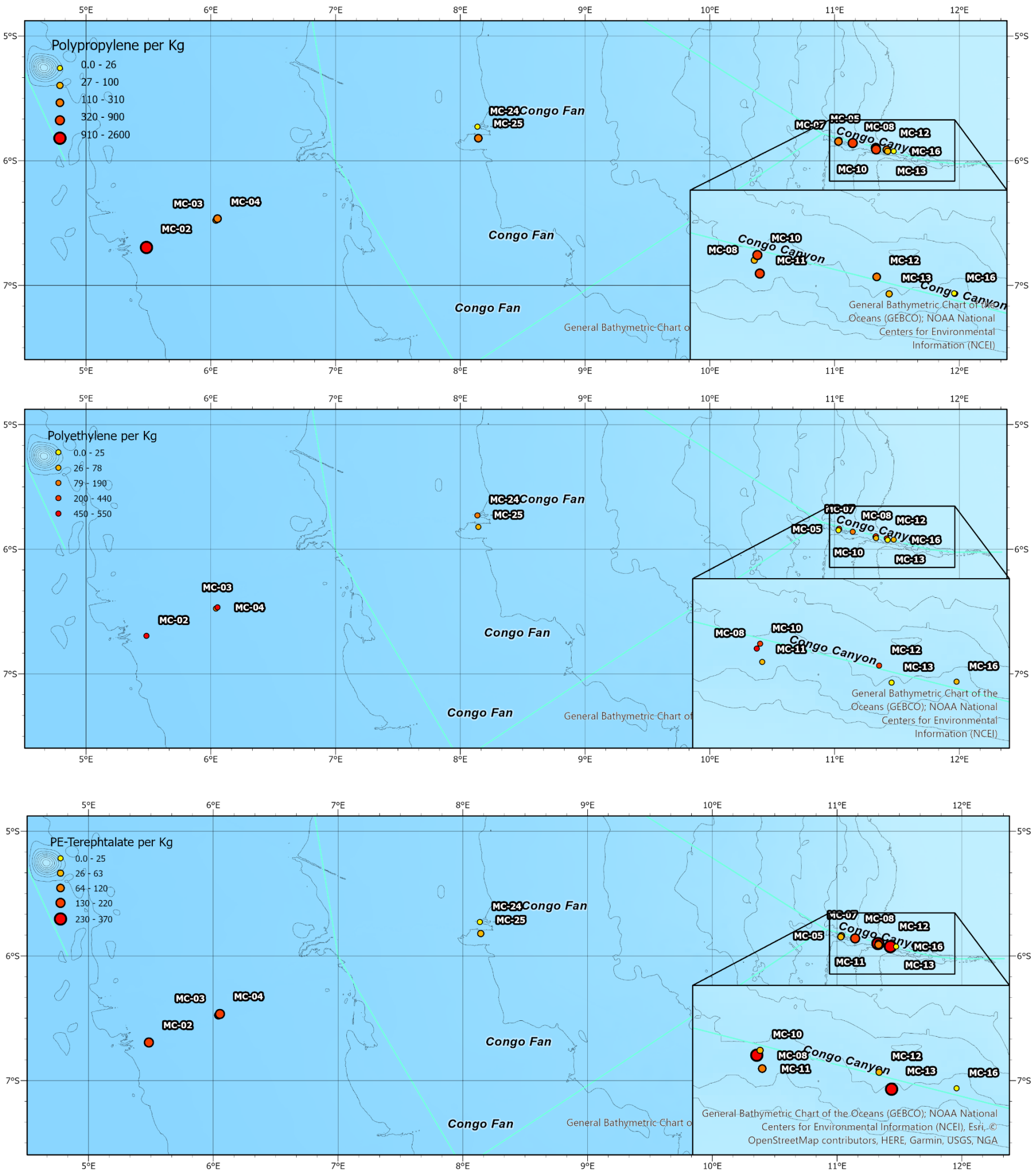

Figure 22 - Comparison of standard deviation of specific polymer load per Kg sediment showing near-shore concentration of PET vs deep water concentration of PP and PE showing preferential deposition of PET in the proximal section of the canyon, whereas less dense plastics are distributed more throughout the system

Particle characteristics

Mean microplastic particle size ranged from 23 µm up to 79 µm, with minimum being 10 µm (the set measuring limit of the analysis program) and largest 476 µm with a gradual decrease in the grainsize of particles at the distal end of the system (Figure 23). Overall, most plastics were either clear with slight tinting, usually yellow, or opaque with an apparent white or black finish, however there was no consistent colouring or staining to indicate a common trend.

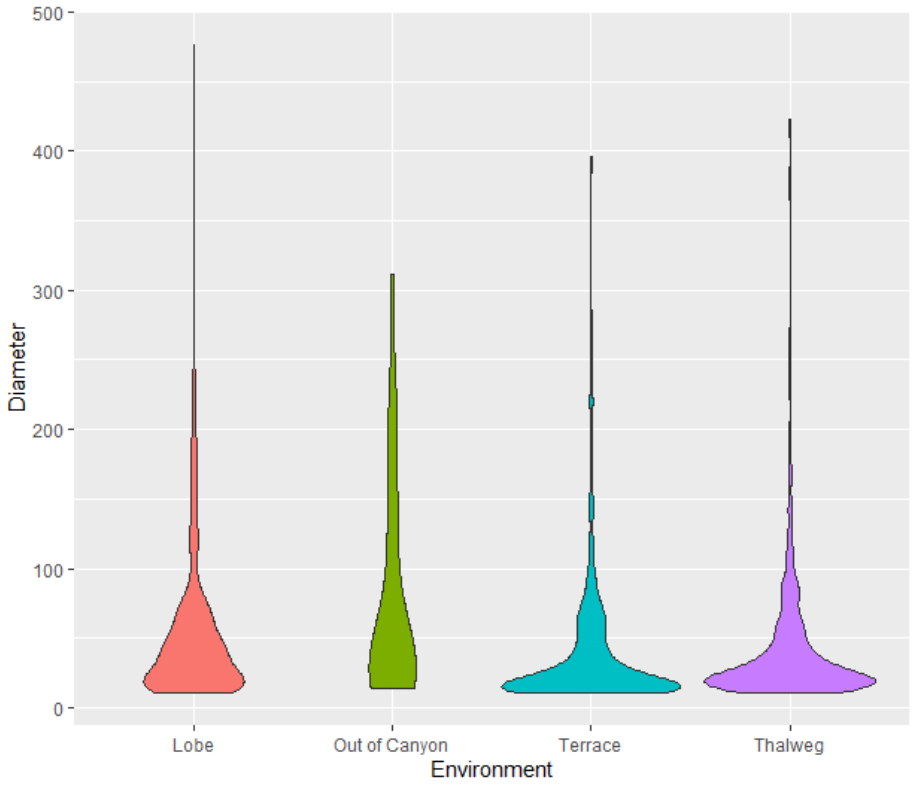

Figure 23 – Violin plot of all measured microplastic particles

Eccentricity of all plastic particles was also evaluated by processing the data to the same workflow as for particle binning, but with the addition of the calculation of mean. Eccentricity ranged from 0.16 to 0.99, mean eccentricity was 0.66. Overall, the particles had a large variation in eccentricity, but most particles are moderately eccentric (Figure 24), and smaller particles were less likely to be eccentric (Figure 25).

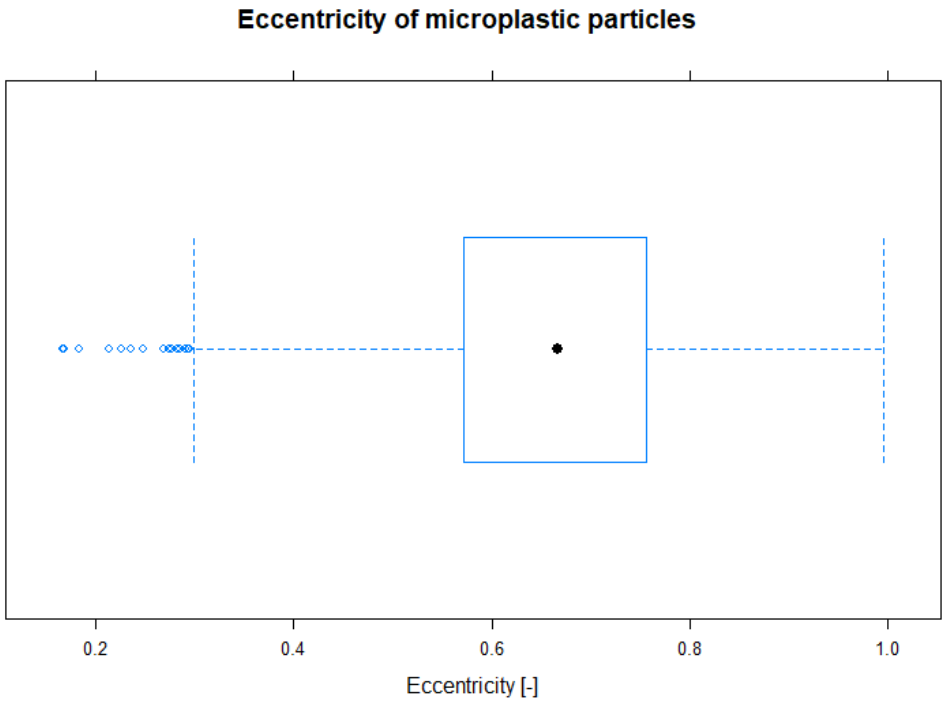

Figure 24 - Graph showing large variations in eccentricity in all measured microplastic particles (quartiles 5th/95th)

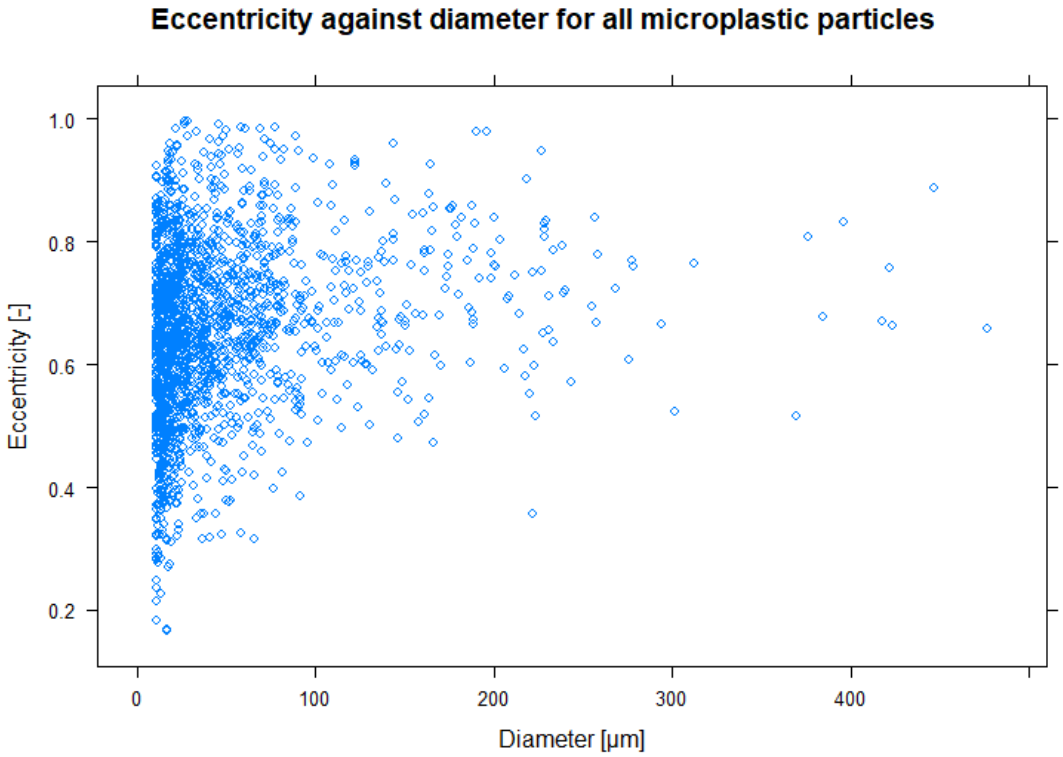

Figure 25 - Comparison of particle eccentricity vs particle diameter for all measured microplastic particles

Variation of grain size across the sub-environments of the Congo Canyon System

Most cores were clay and mud-rich, with the lobe containing the majority of the sandy content. There is a high D_{90} sediment grain size value in the Lobe, and this is apportioned to the presence of organic woody particles, which was not removed from the samples used for sediment grain size analysis.

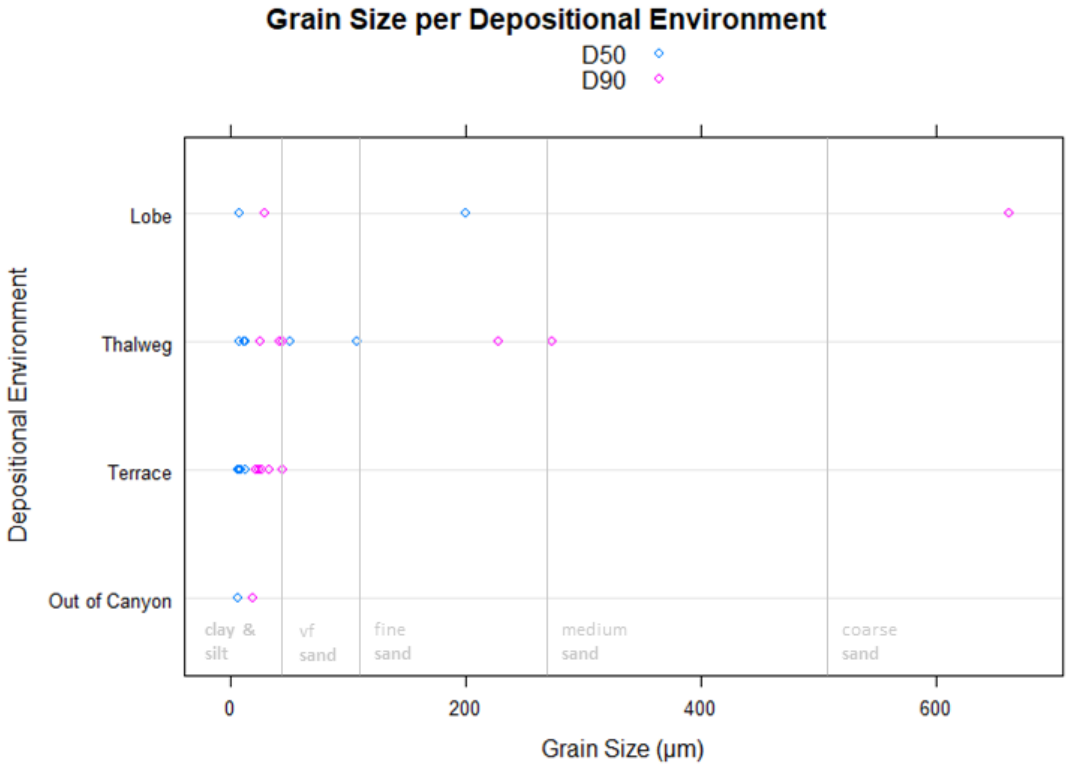

Figure 26 – Measured grain size per depositional environment showing coarser material being deposited on terraces however there is a peak in the lobe due to the entrainment of organic particles

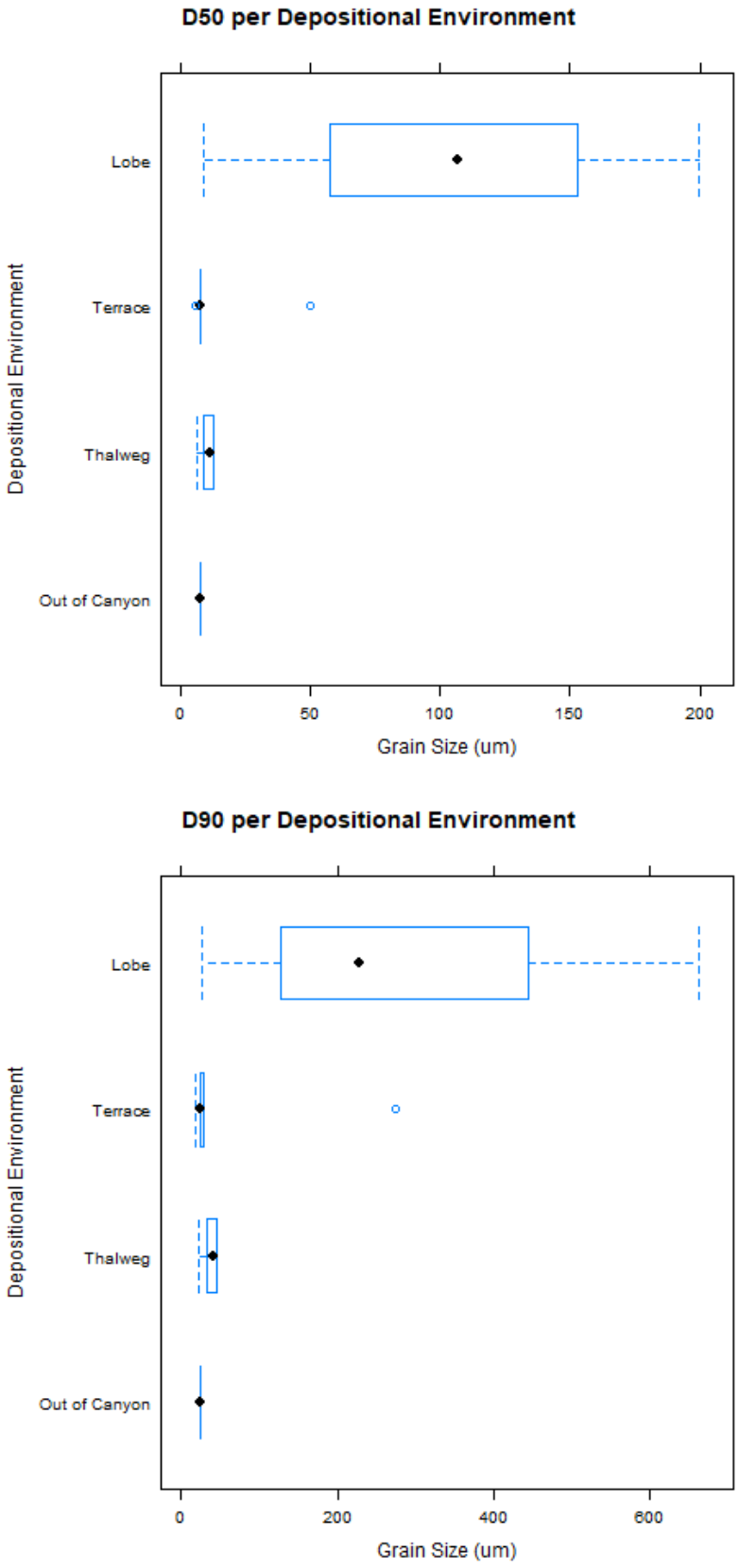

Figure 27 - Box and whisker plots of Grain Size per environment, showing coarsening in distal sediments, n(Lobe) = 2, n(Terrace) = 6, n(Thalweg) = 6, (Out of Canyon) = 1,

Discussions

Refinements to lab protocol

The research of Lopez-Rosales et. al. (2022) was published after the laboratory work for my report was complete, and initially identifies that the protocol used in the laboratory is affected by oversaturation of ethanol. Lopez-Rosales add an additional step of evaporation under controlled conditions (nitrogen rich environment) to deposit a known volume of suspension onto the slides in a controlled, defined manner.

This would have been a beneficial change to the protocol, not only to allow for a known amount of evaporation to allow back-calculation of suspension concentration, but also would have provided better control on the evaporation process.

With regards to slide laying, both Nel *et al.* (2019) and López-Rosales *et al.* (2022) identify a level of operator bias with regard to laying the slides, as there is overall a preference for larger, brighter coloured particles. These are easier to see by the operator laying the slide, and therefore it should be considered that when laying slides, the entirety of the media is exhausted to ensure that the complete slide is imaged.
However, I note that this may result in an excessive number of slides per sample (7-10) which, at current processing rates (10 hours per slide, 11 slides per week) would drastically extend the time taken on the work.

López-Rosales *et al.* (2022) further discussed the issues of setting a strict 'hit rate', as with real-world samples and sediments this can result in misidentification. In comparison, I chose to exclude polymer classes entirely based upon the likelihood of false positive identifications.

This provides a smaller set of data however reduced the number of misidentifications. Overall, López-Roasles et. al. supports the methodology of manually reviewing each 'high quality' hit over the threshold, and therefore it is not currently possible to run a fully automated analysis on microplastic samples.

Relation of polymer to grain size

There is a general trend for lighter plastics to be deposited earlier in the canyon system, and for the denser plastics to remain entrained in the flow and be deposited at the distal reaches. Figure 22 shows that PET, a heavier polymer, is preferentially deposited earlier in the system. Linking with the grain size data (Figure 28) this indicates that the coarser, higher energy sediments at the proximal end of the system are more likely to retain higher density polymers, whereas PP and PE were present throughout the system.

However, the values used are from reference datasets and as such it is not possible to plot a per-particle density graphic.

Relation of plastic density to grain size

The varying energy levels in the canyon system results in different transport processes and this impacts the spatial variation in microplastic load. This is summarised in Figure 19 (p.47).

Enders et al. (2019) investigated the impact of plastic density on the distribution with specific relation to the grain size of the turbidite, and their research indicated that although total microplastic abundance lowers with relation to median sediment grain size (D50), they identified a positive trend whereby increasing grain size realised an increase in higher density plastics.
However this is challenged by Pohl *et al.* (2020) as they indicate that grain size is only related to the trapping of certain particle shapes, especially fibres, and that the distribution of particles is more based upon density, where lighter particles remain buoyant in the flow. This is seen in Figure 22 where high-density PET particles are preferentially trapped at the earlier reaches of the canyon system.

The LDIR's matching library did not discern between high- and low-density variants of polyethylene and polyvinylchloride, as explained in the method. I therefore classified these all as high density due to the average densities as given in Table 5, which may cause particles to be incorrectly assigned to a classification.

I set the density grouping based on the average polymer density being higher or lower than water (1.00 g^{-1} cm^{-3}) following the methodology of Enders et al. (2019) using aggregated polymer database data sourced from material measurements. The plastics and their density groupings can be referred to in Table 5 (overleaf).

Table 5 - List of plastics selected for density comparison

Sign[5]	Polymer name	Average Density[6] (g^{-1} cm^{-3})	Density grouping
PA	Polyamide	1.000 (Nylon 12) - 1.439 (Kevlar) [A]	High
PC	Polycarbonate	1.206 [A]	High
PE	Polyethylene	0.854 [A]	Low
PET	Polyethylene terephthalate	1.333 [A]	High
PMMA	Poly(methyl methyl acrylate)	1.159 [A]	High
PP	Polypropylene	0.861 [A]	Low
PS	Polystyrene	1.052 [A]	High
PTFE	Polytetrafluoroethylene	2.17 [B]	High
PU	Polyurethane	1.052 [B]	High
PVC	Polyvinylchloride	1.388 [A]	High

I plotted the density comparison data together in Figure 28 and this followed the general hypothesis from Enders et. al. that coarser sediments are more likely to contain high density microplastics.

Enders et al consider the ability of mud layers, given the strong static forces, to trap microplastics in the finer elements where total microplastic content is higher, as these contain overall a higher proportion of microplastics and the variance between high- and low-density plastics is harder to discriminate, especially given that in this dataset we have excluded a large number of particles.

I expected grain size to be coarser in the high energy environments (Thalweg) and lower in the distal reaches (Lobe and further) of the system. The grain size data supported this, with a general mud-rich trend in the lower energy sections (Figure 28), however a turbidity current is enriched with mud and so it cannot be assumed that there is a direct correlation between energy level and grain size.

[5] Following ASTM D7611-20 (Resin Identification Code Standard)
[6] Data sources: A: CROW Polymer Database (www.polymerdatabase.com) - B: Scientific Polymer Products Inc. (https://scipoly.com/density-of-polymers-by-density/)

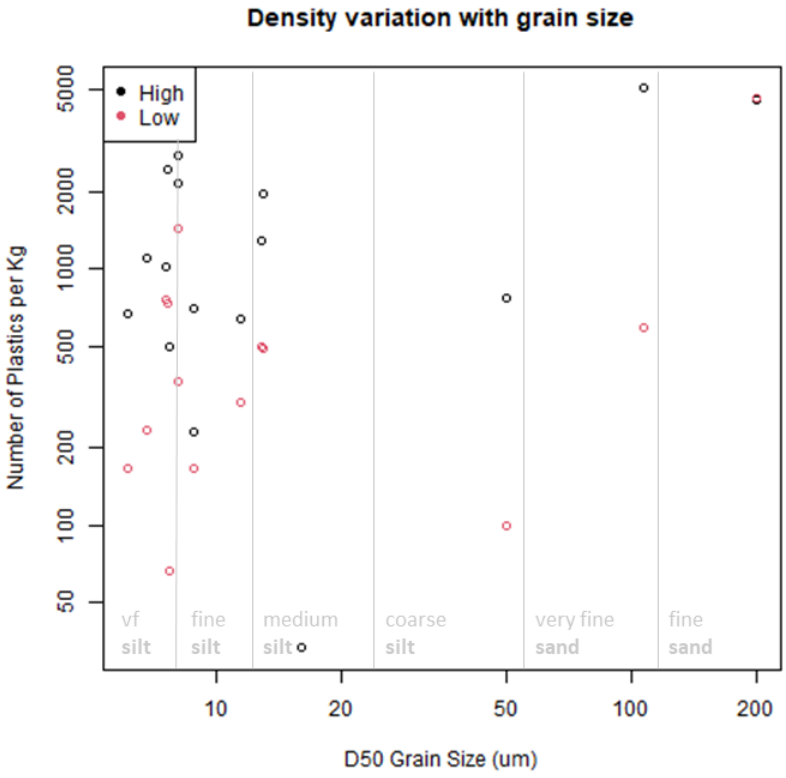

Figure 28 - Comparison of D50 grain size against distribution of low- and high-density plastics

The sample size for which I had to draw conclusions from does not provide for sufficient variation of the findings of Enders et. al., driven primarily by the inability of the LDIR to discern between high density and low-density variations of the same polymer - e.g., High Density Polyethylene (HDPE) vs. Low Density Polyethylene (LDPE).

I noted that Alomar *et al.* (2016) claimed no link between sediment size and microplastic fractions. Their sediments were however shallow in size and show little variation, with microplastic being found up to 2000 µm (2 mm) grain size, which was much larger than the sizes which were available in the Congo Canyon samples. However, I believe their system is biased by samples only being collected from coastal shallow waters, and therefore should have included samples from deeper this would have affected the spread of microplastics.

As can be seen in Table 5a number of the polymers used in this analysis had both high- and low-density applications as this drastically changes the material properties such as tensile and shear strength of the material. Therefore, the response to high energy turbulent flows

for the same type of polymer could be vastly altered, and as such the resulting profile of the microplastic particle gives little to no indication of the original object.

I compared three end member plastics in their spatial distribution, Polypropylene (PP), Polyethylene (PE), and Polyethylene-terephthalate (PET) in Figure 22 (p. 53). PP and PE are low density following the methodology of Enders et al. (2019) whereas PET is high density.

I found PET in greater abundance at the early stages of the system, which indicates this higher density plastic is likely quickly buried and then later reworked, whereas the low density PP and PE remain better distributed at the end of the system, suggesting that they remain entrained within the flows and quickly settle out into the fines at the end of the system.

Additionally, there is a relatively high concentration of microplastics in the terrace deposits (Figure 20 & Figure 21) which indicates a 'pluming' effect, whereby microplastics entrained in the turbidity current are mobile within the sediment body. Eventually these microplastics are liberated from the flow and settle out from the water column into the lower energy environments on the terraces, although it is possible to conclude that these particles may also originate from outside of the turbidity current (Kane and Clare 2019).

Furthermore, both eccentric and spherical particles were examined, and following Pohl *et al.* (2020) it is more likely that the eccentric or fibre-like particles remained within the plume, and therefore it is possible that the less eccentric (i.e., more spherical) particles remain suspended within the flow and are carried further.

Transport of microplastics

While the polymer classes detected in this project – e.g. Polyvinyl Chloride (PVC), Polystyrene (PS), Poly methyl methyl acrylate (PMMA) - correlate with anthropogenic sources, we do not have enough data to define that all are from a riverine source. However, not only are these polymers not naturally occurring, but also the material that is commonly lost at sea consists of 'nurdles' – small primary plastic pellets used in the production of other plastics (Ellinson 2007) - and fishing nets, the latter of which is commonly made of non-natural polyamides such as nylon. Therefore, it is possible to say that the plastics detected are likely both sourced from riverine routes and from direct ocean pollution.

Kane and Clare (2019) note that biological processes have an influence on particles that float on, or are buoyant within, the water column. As the method results in the complete removal of organic matter, it is not possible to evaluate biofouling (Hildebrandt *et al.* 2021). Furthermore, Pierdomenico *et al.* (2020) discuss movement of plastics by thermohaline currents which results in reworking and moving. As the Congo Canyon is located along the coast of West Africa, a heavily used shipping lane, it is highly possible that there is introduction of material from other sources as well as pollution from sea traffic.

The polymers classified in the project cannot be uniquely defined as terrestrial or marine, nor would it be possible to speculate based upon erosional patterns or particle appearance (e.g., colour, shape, eccentricity) the designed purpose of the polymer.
Therefore, although it is likely that microplastics are transported here by the turbidity current, it cannot be excluded that there are additional sources of material input in operation, however comparison of microplastic load of in-canyon cores against the out of canyon sample (S_22) show that there is an increase of microplastic load in the canyon between 2 and 10 times that of the out of canyon system.

Future considerations

Protocol validation

My implementation of the protocol for evaluation of microplastic content was using an existing methodology developed internally at the Helmholtz-Zentrum Hereon. The use of a 'blank' control sample to verify no external contamination is extremely beneficial, however the recovery rate – the volume of plastic material that survives all the processing steps – remains unknown. It may be that numerous fragile plastics are decomposed through any of the seven steps and therefore pass through the filters and are ultimately discarded as waste material.

Validation of the process by using model particles 'spiked' into a given sediment, as undertaken by Cashman *et al.* (2022) would allow us to quantitatively define the success rate of this method, however it is important to ensure that there is no preferential picking of larger particles and that the entire source media is exhausted when laying slides (Nel *et al.* 2019; López-Rosales *et al.* 2022).

Protocol validation could also be used to consider refinements to the method such that used by Cashman *et al.* (2022) where Sodium Bromide at two different densities (1.3 and 1.5 g/cm3) was employed in place of two Zinc Chloride stages used in this project. The use of two different densities may aid in the retention of plastics that have an altered density due to biofouling, as the biofilm is removed during the hypochlorite and peroxide stages which can alter density.

Understanding recovery percentage would also aid in the correction of the bias as mentioned earlier in my thesis, as I understand that there are a number of unknown errors and variances which cannot currently be correctly accounted for.

Behaviour of microbeads in the sediment system

In the course of analysing the slides, I detected small polypropylene particles in the sediment samples analysed, and these are formed in a nearly-perfect spherical shape. These, such as shown in Figure 29 are extremely smooth, and show very little signs of weathering, and are commonly known as microbeads.

Microbeads are most commonly using in cleaning and personal care products for their abrasive nature, and despite their well-documented presence in marine environments and sediments (e.g. Gross 2015; Rillig *et al.* 2017; Shamskhany *et al.* 2021) as well as their harm in living organisms (e.g. Lim 2021; Kwon *et al.* 2022; Liu *et al.* 2022), legislation at a wide-ranging level is still yet to be ratified (e.g. European Chemicals Agency 2021) despite the presence of Microplastics in the UN's Environment Programme, and are subject to substantial lobbying efforts (European Environmental Bureau 2020).

Individual efforts by countries to ban microbeads (e.g. Microbead-Free Waters Act, USA (114th Congress 2015); *The Environmental Protection (Microbeads) (England) Regulations 2017* 2017, French Environmental Code (*Circular Economy Law* 2020)) are limited in power and enforcement potential, and ultimately results in a shifting of microbead products to countries where the law is less enforced or absent. There is therefore no ultimate power or authority that could limit the influx of microbeads into the seas.

The calculations of distribution in the results assume that the distribution of plastics based upon median diameter matches that of the distribution of sediments according to grain size. The canyon is a high energy sedimentary environment and so a wide spectrum of plastic sizes are mobilised, therefore there is a question whether microbeads adhere to the expected fining-upwards of sediments due to energy decrease in a turbidity flow, however as existing experiments (e.g. Pohl *et al.* 2020) do not account for interaction between particles and mud, the impact of the distal ends of the fan in trapping microplastics is not known.

It would be possible to investigate this by dosing a large flume tank with either isotopically tagged microbeads or using microbeads of a sufficiently contrasting colour. Using particles that are iridescent at certain wavelengths would be better than solid colour particles, as this would limit the impact of frictional and decomposition processes in the sediment system, and these could then be imaged with video spectroscopy cameras/software to determine

distribution of the particles after a large scale event, similar to other activities undertaken in the Eurotank (Bell *et al.* 2021). Variations on this could be performed with particles of different shapes and densities to simulate the environment that these particles were deposited in. It would be important to ensure that the microbead material is fully recovered from the flume tank and destroyed to prevent contamination of the environment.

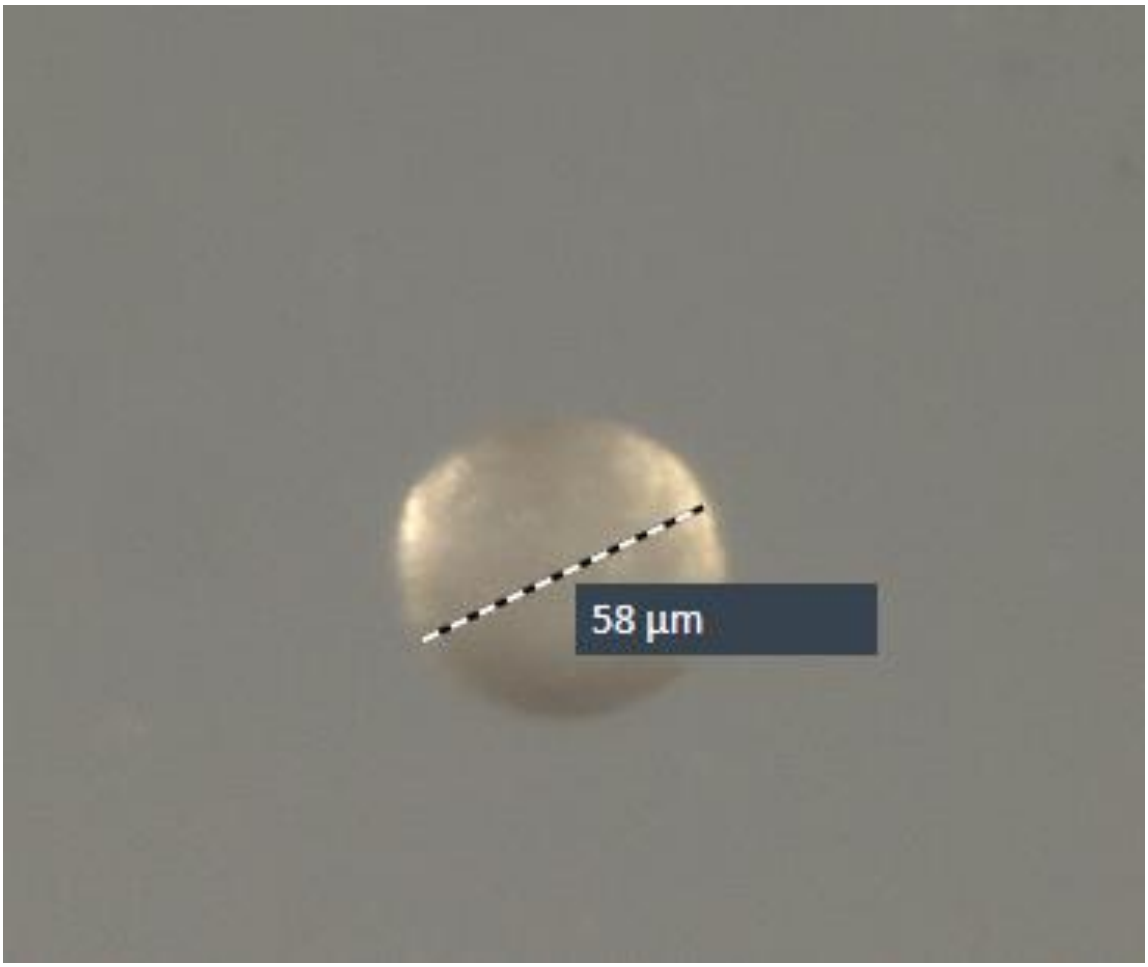

Figure 29 – Polypropylene microbead found in sediment samples

It could also be considered to model the particles in a virtual flume tank/hydrodynamics package, as a high-resolution digital elevation model (DEM) exists and there are a series of flow data measurements known to simulate the environment (Azpiroz-Zabala *et al.* 2017a, b; Pohl *et al.* 2020), however this would also require substantial computing power and knowledge of inter- and intra-particle collisions and interactivity.

Comparison with other locations

A number of sediment traps were deployed as part of the cruise and the samples were recovered. These samples were not analysed as part of this project but continue to be analysed by the Helmholtz-Zentrum Hereon.

Comparison of the data from the sediment traps against the core data would allow for an understanding of the introduction of microplastics into the water column from the turbidity current, and therefore a fuller understanding of the source for microplastics in the Congo Canyon. However, it is possible that the sediment traps also collect microplastics that are already present in the water column. Use of a submersible video capture device could quantify input and residence of plastics, including macro-plastics, and be used to estimate input of material from thermohaline flows.

Furthermore, comparison of these cores against zero-measurements taken on the abyssal plane and open slopes would further correlate the plastic that results from settling from the water column or from movement due to thermohaline currents.

Conclusion

When compared to the original research questions, I can conclude that:

What is the variation in microplastic concentration, size, shape, and polymer-type across different sub environments of the Congo Canyon System?

- Higher density microplastics tend to be found within the coarser, higher energy layers earlier in the system, such as PET being preferentially deposited in the higher energy reaches of the system. But I found that high density plastics are not exclusively present there, and vice versa (Figure 22) as their density affects their retention in the turbidity flow.
- While load varied, with more microplastics being detected in proximal deposits (Figure 20, Figure 21), I find that the size only varied slightly between environments (Figure 23) however further core samples are needed to further qualify this.
- Overall, microplastics can be found throughout the entire Congo Canyon system (Table 3) and I find no solid link between distance from shore and microplastic content (Figure 14).
- Particle eccentricity (Figure 25) and appearance appear to have little to no impact on the behaviour of the particle in a turbidity current, however current flume tank analogues are unable to model the impact of mud on microplastic retention, and so I propose further work on how to explore this (p. 65).

Does the microplastic distribution correlate with the sediment grain size?

- Microplastic concentration only very weakly links to median (D_{50}) and maximum (D_{90}) sediment grain size (Figure 15). However, more microplastics are indicated in the sandier cores (Figure 18) however the sample size (n = 3) may result in this altering after further analyses with the sediment trap data.
- There is no apparent correlation with the work of Enders *et al.* (2019) where higher density plastics match with coarser layers, however there are limitations with the detection capabilities of the equipment and the volume of samples used to corroborate their assumptions, and there is scientific discourse in its comparability with the work of Pohl *et al.* (2020). Ultimately, there is no link between grain size and microplastic abundance found in my work.

What are the possible causes for the distribution pattern of microplastics in a submarine canyon system and could these variations be explained with sediment transport processes?

- The Out of Canyon sample analysed identifies that although there is plastic present out of canyon, this is at concentrations much lower than the plastic in the canyon at 831 microplastics per Kg sediment.
- Plastics in the Congo Canyon are transported by turbidity currents; however, this may not be the only method of transport and we do not have enough data to isolate additional transport methods at present as turbidity flows can entrain material that is already mobile in the water column, and low density particles may settle out from surface plume (p. 63).
- The shape and density of a particle may have influence on the distribution of microplastics in the Congo Canyon, however due to the lack of trustworthy shape data from the LDIR, and given that density data is calculated based upon catalogue data and not real world data, the links made between polymer density and deposition are purely observational.
- The Sediment Trap samples currently being worked on by the Helmholtz-Zentrum Hereon should allow correlation with this dataset to quantify the amount of particles released from the turbidity current, and give further insight into what remains embedded in the flow.
- Additional material input from thermohaline flows cannot be discounted and use of imagery to discriminate plastic input from outside of the turbidity current is needed.

The lab work and analyses have produced a substantial amount of data over multiple modalities giving detailed insight into the occurrence, size, and distribution of microplastics in the Congo Canyon, and I hope that through further analysis and comparison that these can aid in strengthening understanding of microplastic transport in turbidity currents.

Through the publishing of an additional code package (p. 37) I also aim not only to improve the comparability of this dataset, but also to further support research in the field of microplastics, a concern that I consider very important to our future on this planet.

Bibliography

Alomar, C., Estarellas, F. and Deudero, S. 2016. Microplastics in the Mediterranean Sea: Deposition in coastal shallow sediments, spatial variation and preferential grain size. *Marine Environmental Research*, **115**, 1–10, https://doi.org/10.1016/j.marenvres.2016.01.005.

Araujo, C.F., Nolasco, M.M., Ribeiro, A.M.P. and Ribeiro-Claro, P.J.A. 2018. Identification of microplastics using Raman spectroscopy: Latest developments and future prospects. *Water Research*, **142**, 426–440, https://doi.org/10.1016/j.watres.2018.05.060.

Arthur, C., Baker, J., et al. 2008. Summary of the International Research Workshop on the Occurrence, Effects, and Fate of Microplastic Marine Debris. *In*: Arthur, C., Baker, J. and Bamford, H. (eds) *Proceedings of the International Research Workshop on the Occurrence, Effects, and Fate of Microplastic Marine Debris*.

Azpiroz-Zabala, M., Cartigny, M.J.B., Sumner, E.J., Clare, M.A., Talling, P.J., Parsons, D.R. and Cooper, C. 2017a. A General Model for the Helical Structure of Geophysical Flows in Channel Bends. *Geophysical Research Letters*, **44**, 11,932-11,941, https://doi.org/10.1002/2017GL075721.

Azpiroz-Zabala, M., Cartigny, M.J.B., et al. 2017b. Newly recognized turbidity current structure can explain prolonged flushing of submarine canyons. *Science Advances*, **3**, https://doi.org/10.1126/sciadv.1700200.

Bell, D., Soutter, E.L., Cumberpatch, Z.A., Ferguson, R.A., Spychala, Y.T., Kane, I.A. and Eggenhuisen, J.T. 2021. Flow-process controls on grain type distribution in an experimental turbidity current deposit: Implications for detrital signal preservation and microplastic distribution in submarine fans. *The Depositional Record*, **7**, 392–415, https://doi.org/10.1002/dep2.153.

Borges-Ramírez, M.M., Mendoza-Franco, E.F., Escalona-Segura, G. and Osten, J.R. 2020. Plastic density as a key factor in the presence of microplastic in the gastrointestinal tract of commercial fishes from Campeche Bay, Mexico. *Environmental Pollution*, **267**, 115659, https://doi.org/10.1016/j.envpol.2020.115659.

Cantwell, M. 2020. Deep-sea currents are behind the ocean's thickest piles of microplastics. *Science*, https://doi.org/10.1126/science.abd3039.

Carpenter, E.J. and Smith, K.L. 1972. Plastics on the Sargasso sea surface. *Science (New York, N.Y.)*, **175**, 1240–1241, https://doi.org/10.1126/science.175.4027.1240.

Cashman, M.A., Langknecht, T., El Khatib, D., Burgess, R.M., Boving, T.B., Robinson, S. and Ho, K.T. 2022. Quantification of microplastics in sediments from Narragansett Bay, Rhode Island USA using a novel isolation and extraction method. *Marine Pollution Bulletin*, **174**, 113254, https://doi.org/10.1016/j.marpolbul.2021.113254.

Cole, M., Lindeque, P., Fileman, E., Halsband, C., Goodhead, R., Moger, J. and Galloway, T.S. 2013. Microplastic Ingestion by Zooplankton. *Environmental Science & Technology*, **47**, 6646–6655, https://doi.org/10.1021/es400663f.

Coppock, R.L., Cole, M., Lindeque, P.K., Queirós, A.M. and Galloway, T.S. 2017. A small-scale, portable method for extracting microplastics from marine sediments. *Environmental Pollution*, **230**, 829–837, https://doi.org/10.1016/j.envpol.2017.07.017.

Coppock, R.L., Lindeque, P.K., et al. 2021. Benthic fauna contribute to microplastic sequestration in coastal sediments. *Journal of Hazardous Materials*, **415**, 125583, https://doi.org/10.1016/j.jhazmat.2021.125583.

Costa, P.J.M. 2016. Sediment Transport. *Encyclopedia of Estuaries*, 562–567, https://doi.org/10.1007/978-94-017-8801-4_187.

Dennielou, B., Droz, L., et al. 2017. Morphology, structure, composition and build-up processes of the active channel-mouth lobe complex of the Congo deep-sea fan with inputs from remotely operated underwater vehicle (ROV) multibeam and video surveys. *Deep Sea Research Part II: Topical Studies in Oceanography*, **142**, 25–49, https://doi.org/10.1016/j.dsr2.2017.03.010.

El-Gareb, F.R. 2021. *Optimization of a Microplastic Sample Preparation Protocol for Laser Direct Infrared Imaging (LDIR) Measurements to Analyze Microplastic Occurrence and Distribution along a Transect in the Indian Ocean*. Universität Hamburg.

Ellinson, K. 2007. The trouble with nurdles. *Frontiers in Ecology and the Environment*, **5**, 396–396, https://doi.org/10.1890/1540-9295%282007%295%5B396%3ATTWN%5D2.0.CO%3B2.

Enders, K., Käppler, A., et al. 2019. Tracing microplastics in aquatic environments based on sediment analogies. *Scientific Reports*, **9**, https://doi.org/10.1038/s41598-019-50508-2.

European Environmental Bureau. 2020. *EU Microplastics Ban: How Industry Pressure Led the European Chemicals Agency to Dilute Its Proposals*.

Faist, J., Capasso, F., Sivco, D.L., Sirtori, C., Hutchinson, A.L. and Cho, A.Y. 1994. Quantum Cascade Laser. *Science*, **264**, 553–556, https://doi.org/10.1126/science.264.5158.553.

Gardner, W.D., Glover, L.K. and Hollister, C.D. 1980. Canyons off northwest Puerto Rico: Studies of their origin and maintenance with the nuclear research submarine NR-1. *Marine Geology*, **37**, 41–70, https://doi.org/10.1016/0025-3227(80)90011-0.

Garzanti, E., Bayon, G., Dennielou, B., Barbarano, M., Limonta, M. and Vezzoli, G. 2021. The Congo deep-sea fan: Mineralogical, REE, and Nd-isotope variability in quartzose passive-margin sand. *Journal of Sedimentary Research*, **91**, 433–450, https://doi.org/10.2110/jsr.2020.100.

Geyer, R., Jambeck, J.R. and Law, K.L. 2017. Production, use, and fate of all plastics ever made. *Science Advances*, **3**, https://doi.org/10.1126/sciadv.1700782.

Gross, M. 2015. Oceans of plastic waste. *Current Biology*, **25**, R93–R96, https://doi.org/10.1016/j.cub.2015.01.038.

Hansen, B. 2021. *Request to the Committee for Risk Assessment to Prepare a Supplementary Opinion on the Restriction Dossier on Intentionally-added Microplastics,* European Chemicals Agency, **I(2021)0013**, https://echa.europa.eu/documents/10162/17090/rac_mandate_follow_up_microplastics_en.pdf.

Hartmann, N.B., Hüffer, T., et al. 2019. Are We Speaking the Same Language? Recommendations for a Definition and Categorization Framework for Plastic Debris. *Environmental Science & Technology*, **53**, 1039–1047, https://doi.org/10.1021/acs.est.8b05297.

Harvey, G.R., Bowen, V.T., Backus, R.H. and Grice, G.D. 1971. Chlorinated Hydrocarbons in Open-Ocean Atlantic Organisms. *In*: Dyrssen, D. (ed.) *The Changing Chemistry of the Oceans : Proceedings of the 20th Nobel Symposium*.

Hay, W.W. 2016. Submarine Canyons. *In*: *Encyclopedia of Marine Geosciences*. 807–808., https://doi.org/10.1007/978-94-007-6238-1_150.

Hildebrandt, L., El-Gareb, F., Zimmerman, T., Klein, O., Emeis, K.-C., Proefrock, D. and Kerstan, A. 2020. *Fast, Automated Microplastics Analysis Using Laser Direct Chemical Imaging (Application Note: Environmental Water Analysis)*.

Hildebrandt, L., El Gareb, F., Zimmermann, T., Klein, O., Kerstan, A., Emeis, K.-C. and Pröfrock, D. 2021. Spatial Distribution of Microplastics in the Tropical Indian Ocean Based on Laser Direct Infrared Imaging and Microwave-Assisted Matrix Digestion. *SSRN Electronic Journal*, https://doi.org/10.2139/ssrn.3961974.

Jambeck, J.R., Geyer, R., et al. 2015. Plastic waste inputs from land into the ocean. *Science*, **347**, 768–771, https://doi.org/10.1126/science.1260352.

Jones, E.S., Ross, S.W., Robertson, C.M. and Young, C.M. 2022. Distributions of microplastics and larger anthropogenic debris in Norfolk Canyon, Baltimore Canyon, and the adjacent continental slope (Western North Atlantic Margin, U.S.A.). *Marine Pollution Bulletin*, **174**, 113047, https://doi.org/10.1016/j.marpolbul.2021.113047.

Kane, I.A. and Clare, M.A. 2019. Dispersion, Accumulation, and the Ultimate Fate of Microplastics in Deep-Marine Environments: A Review and Future Directions. *Frontiers in Earth Science*, **7**, https://doi.org/10.3389/feart.2019.00080.

Kane, I.A., Clare, M.A., Miramontes, E., Wogelius, R., Rothwell, J.J., Garreau, P. and Pohl, F. 2020. Seafloor microplastic hotspots controlled by deep-sea circulation. *Science*, **368**, 1140–1145, https://doi.org/10.1126/science.aba5899.

Karlsson, T.M., Kärrman, A., Rotander, A. and Hassellöv, M. 2020. Comparison between manta trawl and in situ pump filtration methods, and guidance for visual identification of microplastics in surface waters. *Environmental Science and Pollution Research*, **27**, 5559–5571, https://doi.org/10.1007/s11356-019-07274-5.

Klaucke, I., Hesse, R. and Ryan, W.B.F. 1998. Morphology and structure of a distal submarine trunk channel: The Northwest Atlantic Mid-Ocean Channel between lat 53°N and 44°30′N. *Geological Society of America Bulletin*, **110**, 22–34, https://doi.org/10.1130/0016-7606(1998)110<0022:MASOAD>2.3.CO;2.

Kwon, W., Kim, D., et al. 2022. Microglial phagocytosis of polystyrene microplastics results in immune alteration and apoptosis in vitro and in vivo. *Science of The Total Environment*, **807**, 150817, https://doi.org/10.1016/j.scitotenv.2021.150817.

L'Assemblée nationale et le Sénat (FR). 2020. *Loi N° 2020-105 Relative à La Lutte Contre Le Gaspillage et à l'économie Circulaire (Law No. 2020-105 Regarding a Circular Economy and the Fight Against Waste)*. **2020–105**, https://www.legifrance.gouv.fr/jorf/id/JORFTEXT000041553759/.

Leeson, C. 2016. *A Plastic Ocean*, https://aplasticocean.movie/.

Lim, X. 2021. Microplastics are everywhere — but are they harmful? *Nature*, **593**, 22–25, https://doi.org/10.1038/d41586-021-01143-3.

Liu, L., Xu, M., Ye, Y. and Zhang, B. 2022. On the degradation of (micro)plastics: Degradation methods, influencing factors, environmental impacts. *Science of The Total Environment*, **806**, 151312, https://doi.org/10.1016/j.scitotenv.2021.151312.

Löder, M.G.J.J. and Gerdts, G. 2015. Methodology Used for the Detection and Identification of Microplastics—A Critical Appraisal. *In*: *Marine Anthropogenic Litter*. 201–227., https://doi.org/10.1007/978-3-319-16510-3_8.

López-Rosales, A., Andrade, J., Fernández-González, V., López-Mahía, P. and Muniategui-Lorenzo, S. 2022. A reliable method for the isolation and characterization of microplastics in fish gastrointestinal tracts using an infrared tunable quantum cascade laser system. *Marine Pollution Bulletin*, **178**, 113591, https://doi.org/10.1016/j.marpolbul.2022.113591.

Luo, X., Wang, Z., Yang, L., Gao, T. and Zhang, Y. 2022. A review of analytical methods and models used in atmospheric microplastic research. *Science of The Total Environment*, **828**, 154487, https://doi.org/10.1016/j.scitotenv.2022.154487.

Nel, H.A., Dalu, T., Wasserman, R.J. and Hean, J.W. 2019. Colour and size influences plastic microbead underestimation, regardless of sediment grain size. *Science of the Total Environment*, **655**, 567–570, https://doi.org/10.1016/j.scitotenv.2018.11.261.

Ocamringa, C. 2021. Plastic waste in Kinshasa's river. *Global 3000 - The Globalization Programme,* https://p.dw.com/p/3zskW.

Pierdomenico, M., Casalbore, D. and Chiocci, F.L. 2019. Massive benthic litter funnelled to deep sea by flash-flood generated hyperpycnal flows. *Scientific Reports*, **9**, 5330, https://doi.org/10.1038/s41598-019-41816-8.

Pierdomenico, M., Casalbore, D. and Chiocci, F.L. 2020. The key role of canyons in funnelling litter to the deep sea: A study of the Gioia Canyon (Southern Tyrrhenian Sea). *Anthropocene*, **30**, 100237, https://doi.org/10.1016/j.ancene.2020.100237.

Pohl, F., Eggenhuisen, J.T., Kane, I.A. and Clare, M.A. 2020. Transport and Burial of Microplastics in Deep-Marine Sediments by Turbidity Currents. *Environmental Science & Technology*, **54**, 4180–4189, https://doi.org/10.1021/acs.est.9b07527.

Primpke, S., Fischer, M., Lorenz, C., Gerdts, G. and Scholz-Böttcher, B.M. 2020. Comparison of pyrolysis gas chromatography/mass spectrometry and hyperspectral FTIR imaging spectroscopy for the analysis of microplastics. *Analytical and Bioanalytical Chemistry*, **412**, 8283–8298, https://doi.org/10.1007/s00216-020-02979-w.

Rillig, M.C., Ziersch, L. and Hempel, S. 2017. Microplastic transport in soil by earthworms. *Scientific Reports*, **7**, https://doi.org/10.1038/s41598-017-01594-7.

Samandra, S., Johnston, J.M., et al. 2022. Microplastic contamination of an unconfined groundwater aquifer in Victoria, Australia. *Science of the Total Environment*, **802**, https://doi.org/10.1016/j.scitotenv.2021.149727.

Scircle, A., Cizdziel, J. V., Tisinger, L., Anumol, T. and Robey, D. 2020. Occurrence of Microplastic Pollution at Oyster Reefs and Other Coastal Sites in the Mississippi Sound, USA: Impacts of Freshwater Inflows from Flooding. *Toxics*, **8**, 35, https://doi.org/10.3390/toxics8020035.

Secretary of State of the United Kingdom. 2017. *The Environmental Protection (Microbeads) (England) Regulations 2017*. **1312**, https://www.legislation.gov.uk/uksi/2017/1312.

Selley, R.C. 2000. *Applied Sedimentology*, 2nd ed., ISBN: 9780126363753.

Shamskhany, A., Li, Z., Patel, P. and Karimpour, S. 2021. Evidence of Microplastic Size Impact on Mobility and Transport in the Marine Environment: A Review and Synthesis of Recent Research. *Frontiers in Marine Science*, **8**, https://doi.org/10.3389/fmars.2021.760649.

Shepard, F.P. 1951. Transporation of Sand into Deep Water. *In*: Hough, J. L. (ed.) *Turbidity Currents and the Transporation of Coarse Sediments to Deep Water*. 53–65.

Slomkowski, S., Alemán, J. V., et al. 2011. Terminology of polymers and polymerization

processes in dispersed systems (IUPAC Recommendations 2011). *Pure and Applied Chemistry*, **83**, 2229–2259, https://doi.org/10.1351/PAC-REC-10-06-03.

Stow, D.A.V. 1994. Deep sea processes of sediment transport and deposition. *In*: Pye, K. (ed.) *Sediment Transport and Depositional Processes*. 257–291.

Talling, P., Baker, M., et al. 2022. Flood and tides trigger longest measured sediment flow that accelerates for thousand kilometers into deep-sea. *Nature Portfolio (preprint)*, https://doi.org/10.21203/rs.3.rs-1181750%2Fv1.

US Congress. 2015. *Microbead-Free Waters Act of 2015*. **3129**, https://www.congress.gov/bill/114th-congress/house-bill/1321.

Verschoor, A.J. 2015. *Towards a Definition of Microplastics: Considerations for the Specification of Physico-Chemical Properties*, Rijksinstituut voor Volksgezondheid en Millieu, Bilthoven, Netherlands, https://www.rivm.nl/bibliotheek/rapporten/2015-0116.pdf.

von Moos, N., Burkhardt-Holm, P. and Köhler, A. 2012. Uptake and Effects of Microplastics on Cells and Tissue of the Blue Mussel Mytilus edulis L. after an Experimental Exposure. *Environmental Science & Technology*, **46**, 11327–11335, https://doi.org/10.1021/es302332w.

Zhong, G. and Peng, X. 2021. Transport and accumulation of plastic litter in submarine canyons—The role of gravity flows. *Geology*, **49**, 581–586, https://doi.org/10.1130/G48536.1.

Appendices

Appendix I: List of Materials

Equipment	Quantity	Manufacturer	Part code
Glass flask c. 0.5L	3	Custom made	n/a
PTFE Stirring Rod; 15mm 9mm	 3 3	Non-specific	Unknown
Filter stem	3	Merck Millipore	XX1514702
Filter clamp	3	Merck Millipore	XX1004703
Filter funnel	3	Merck Millipore	XX1014707
Separatory funnel, 100 mL	3	Non-specific	Unknown
Filter; PTFE, 5 µm Polycarbonate, 0.4 µm Glass fibre, 1.2 µm	 12 (min.) 5 (min.) 5 (min.)	 Sartorius Sartorius Merck Millipore	 11842--47------N 23006--47------N APFC04700
Zinc Chloride, powder	3 Kg	Sigma Aldrich	208086
Ethanol 96% pure	5 Litres	Carl Roth GmbH	P075.5
Sodium Hypochlorite 10%	1 Litre	PanReac AppliChem (ITW Reagents)	211921.1211
TXL Cellulase	500 mL	ASA Spezialenzyme GmbH	3015
pH Buffer Solution (CH3COOH + CH3COONa)	500 mL	Made in-house (c = 1.00 mol L^{-1}, pH = 5)	n/a
Hydrogen Peroxide, 30%	500 mL	Carl Roth GmbH	9681.1
Nalgene FEP Squirt bottle	5	ThermoFisher Scientific	2403-0500
Flat cover slip forceps	1	Carl Roth GmbH	K719.1
Glass analytical funnel	1	Carl Roth GmbH	K246.1
Borosilicate pipette; 5 mL 25 mL	 1 5	 Carl Roth GmbH Carl Roth GmbH	 AH40.1 HXX0.1
Borosilicate beakers; 250 mL 1 L	 3 1	Non-specific	Unknown
Glass Petri Dish: 35mm diameter 65mm diameter	 3 12	Non-specific	Unknown
Brown glass reagent bottles, 1L, with FEP screw caps	4	Non-specific	Unknown
Discover SP-D supplies: Quartz Vessel, 35 mL ActiVent caps	 3 3	 CEM, Incorporated CEM, Incorporated	 909780 909350
Baysilone Silicone Paste	1	GE Bayer Silicones	No longer available[7]

[7] Now produced by Kurt Obermeier GmbH & Co. KG as Korasilon® with product code M-S 2-270

Appendix II: Microplastic diameters per sample

Note: Whiskers are at 5th and 95th quartiles

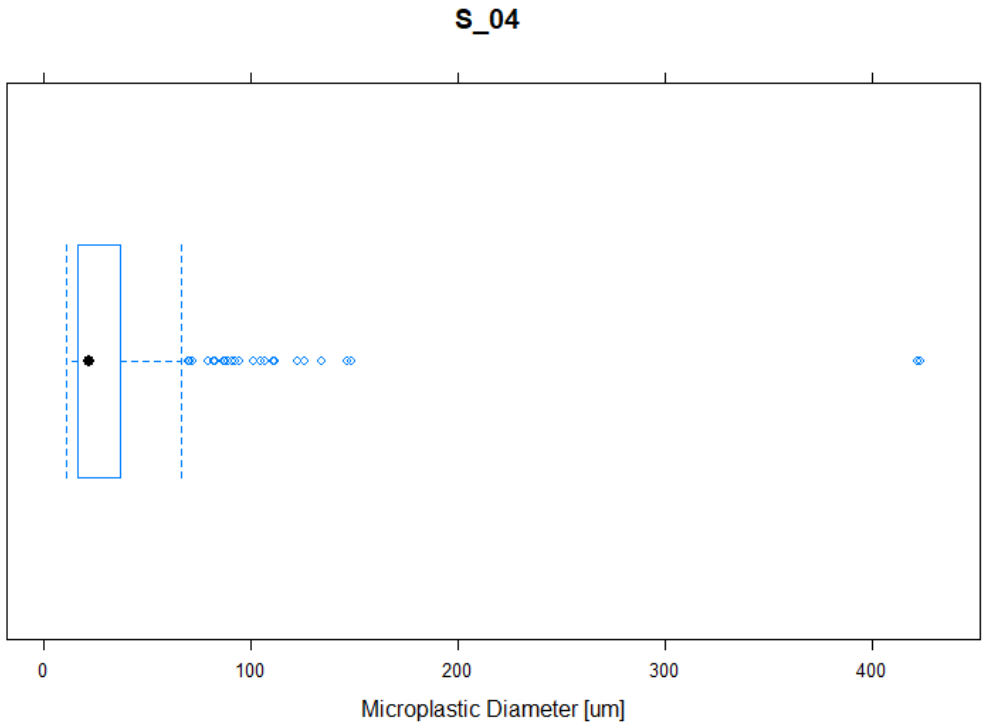

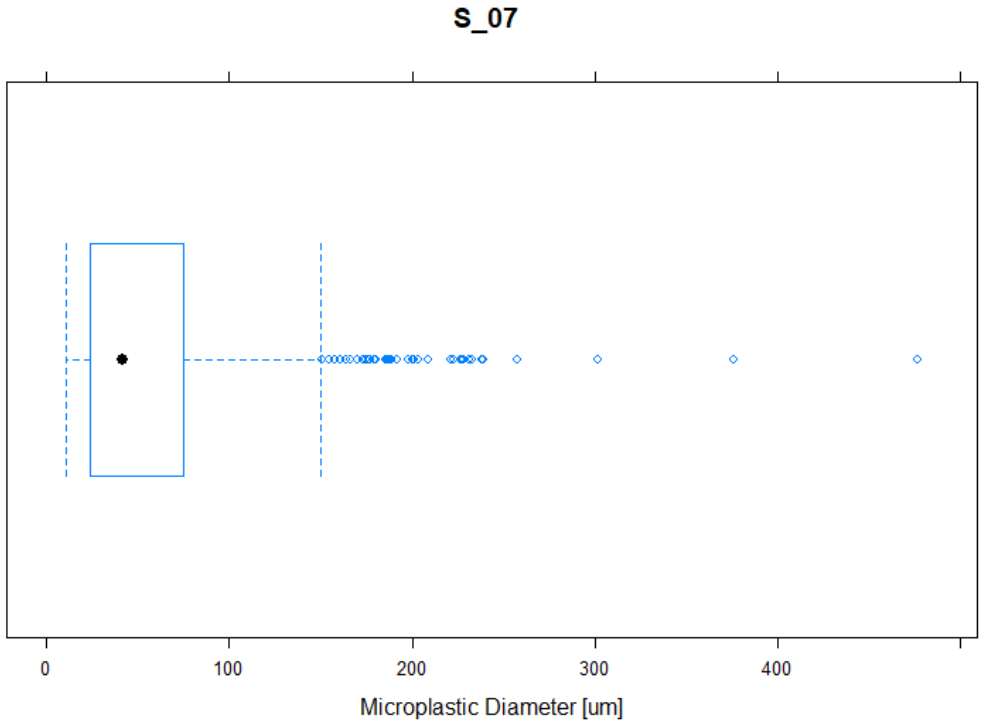

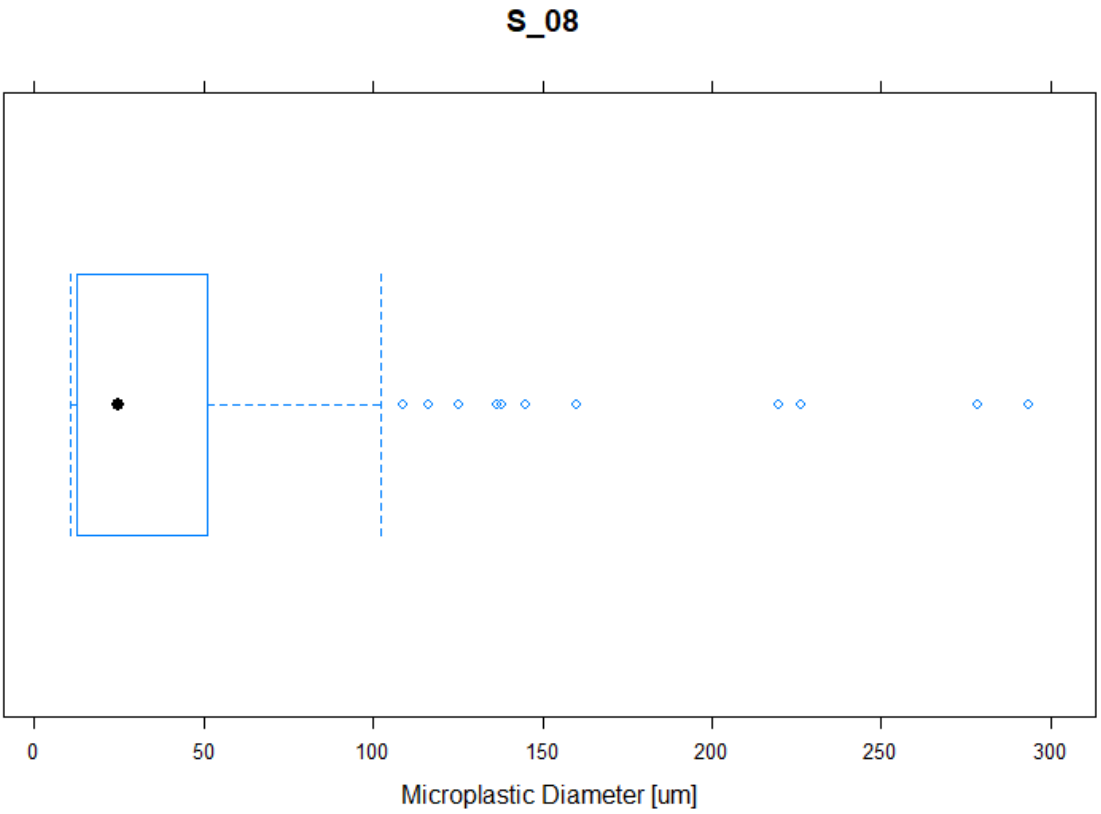
S_08
0
50
100
150
200
250
300
Microplastic Diameter [um]

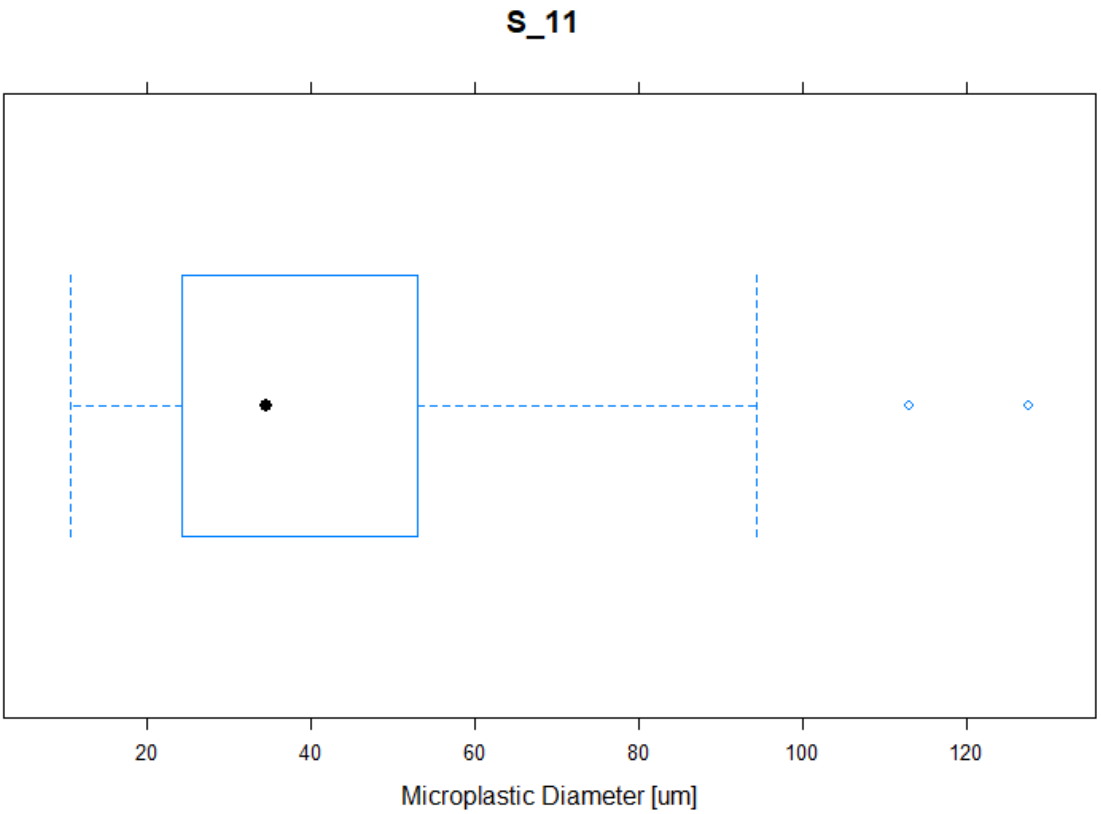
S_11
20
40
60
80
100
120
Microplastic Diameter [um]

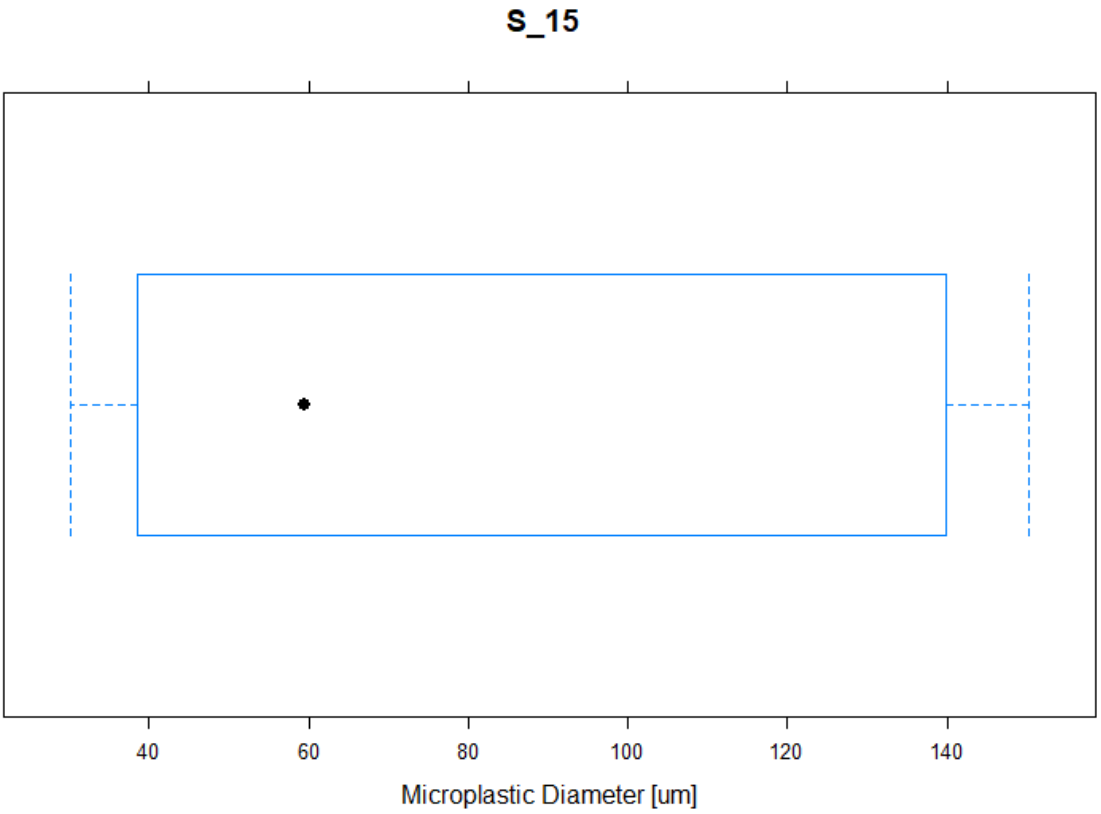
S_15
40
60
80
100
120
140
Microplastic Diameter [um]

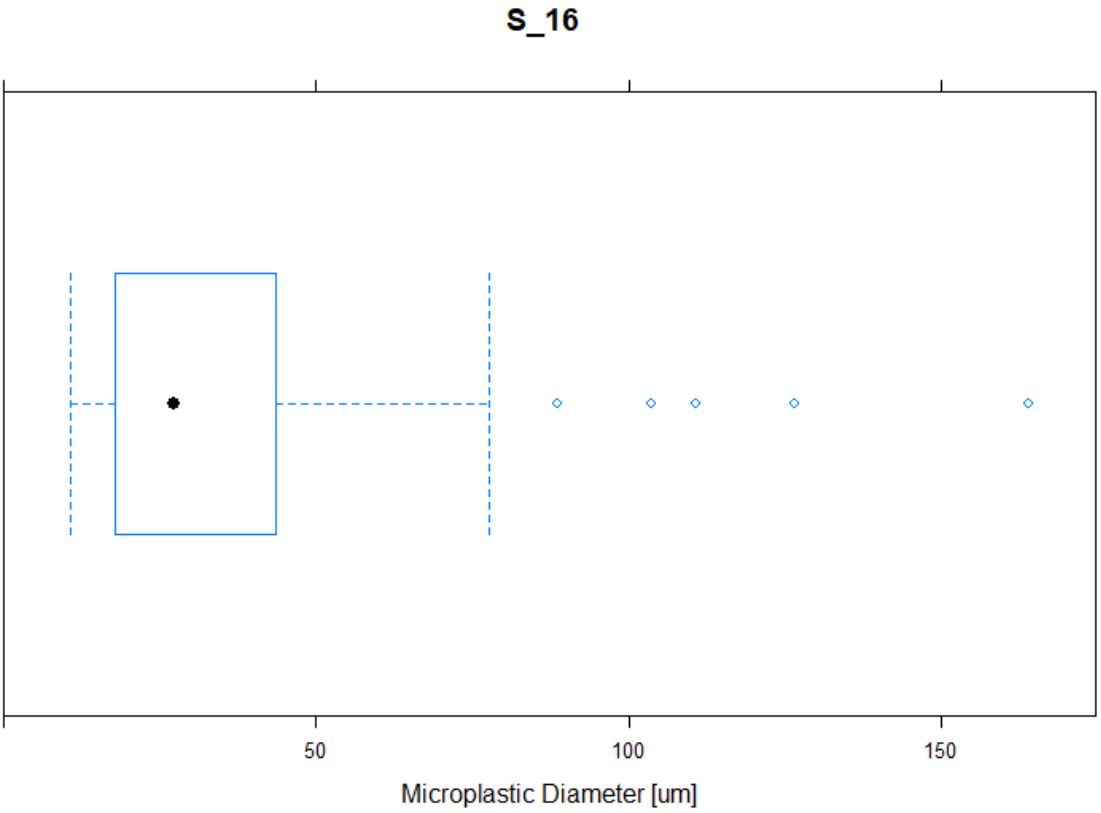
S_16
50
100
150
Microplastic Diameter [um]

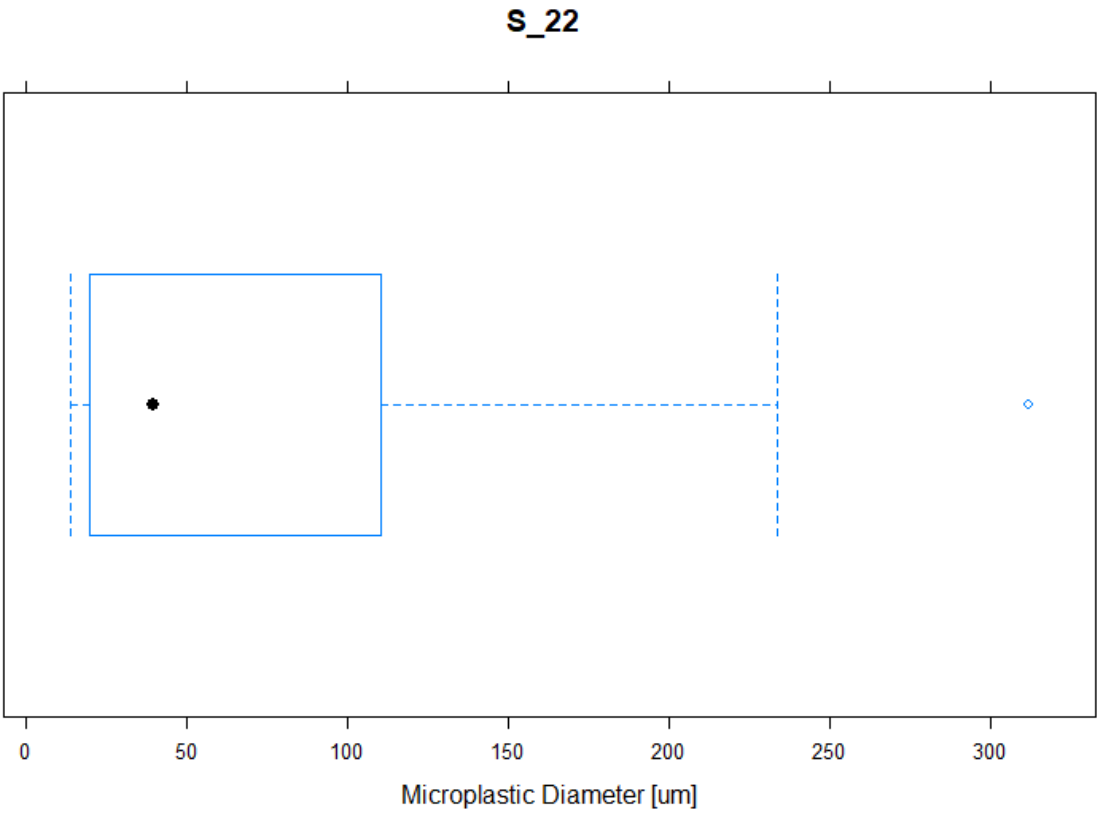
S_22
0
50
100
150
200
250
300
Microplastic Diameter [um]

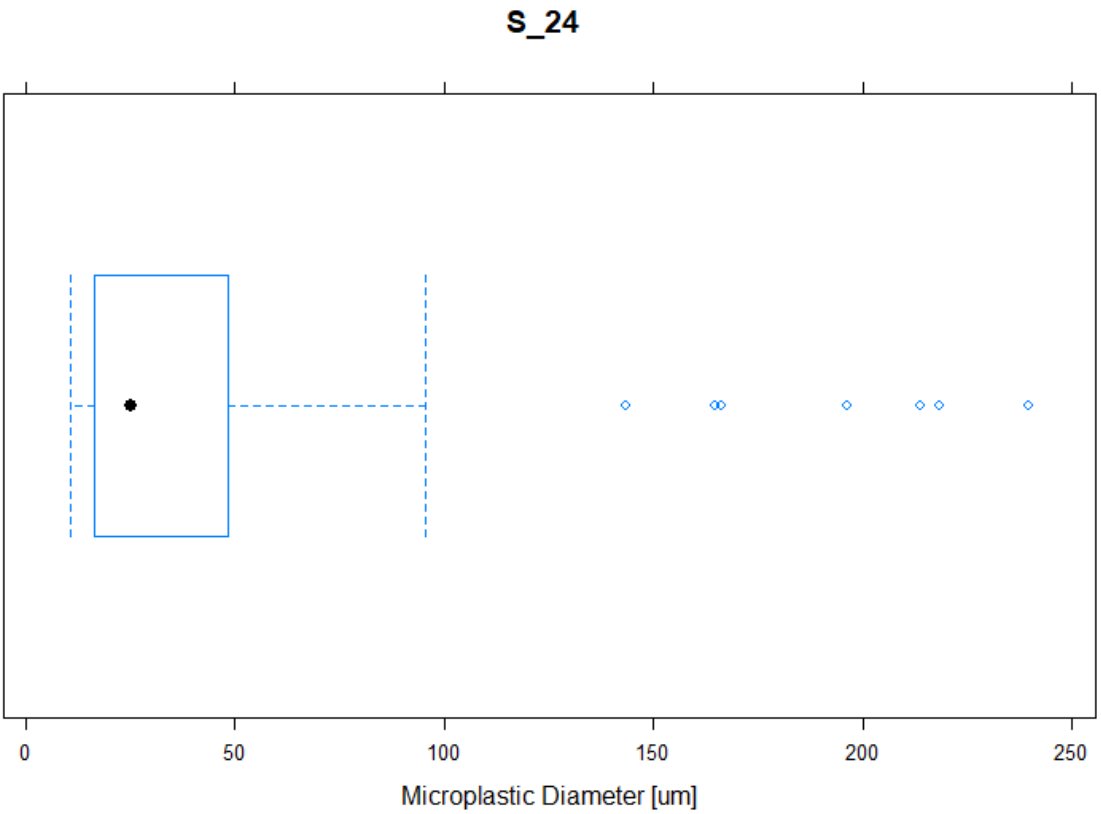
S_24
0
50
100
150
200
250
Microplastic Diameter [um]

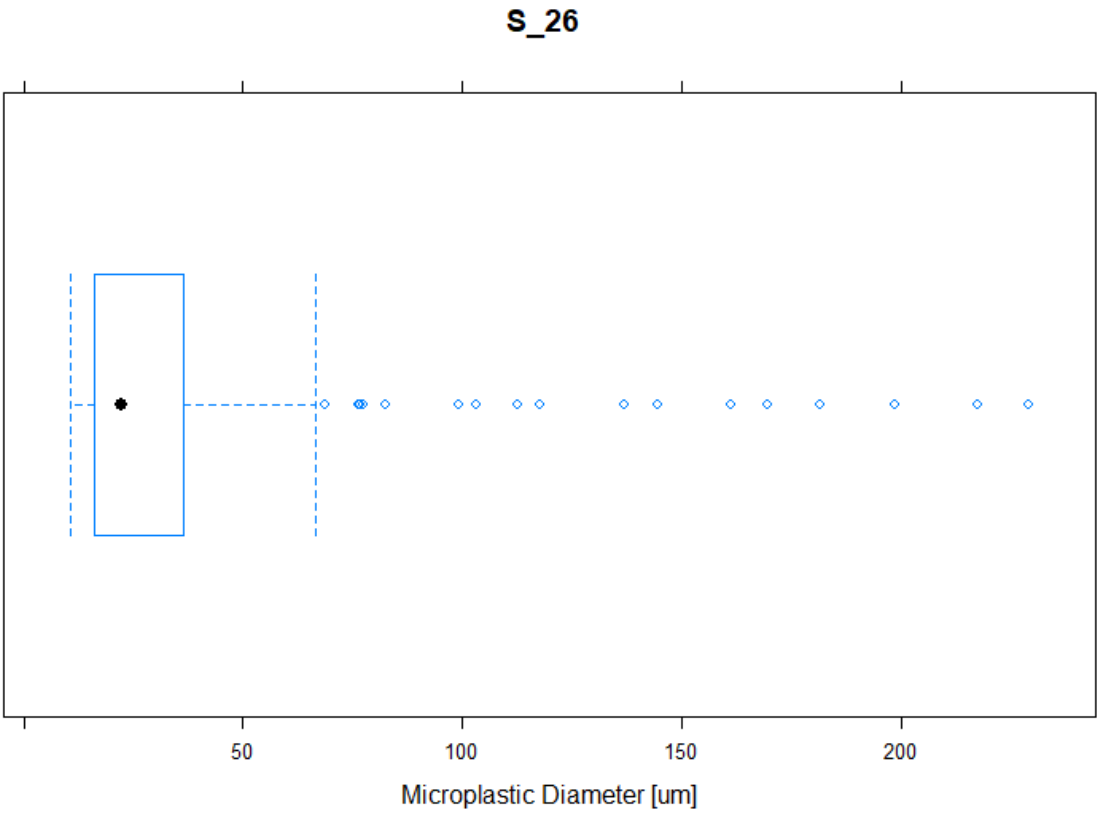
S_26
50
100
150
200
Microplastic Diameter [um]

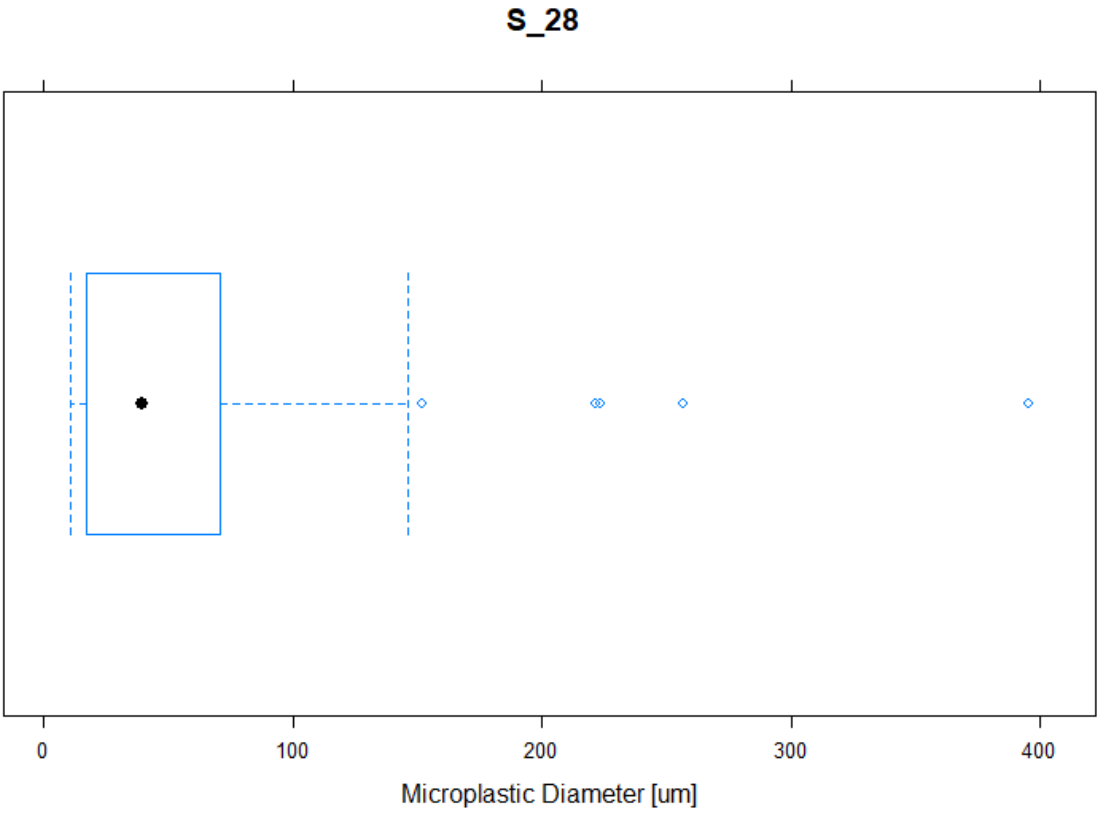
S_28
0
100
200
300
400
Microplastic Diameter [um]

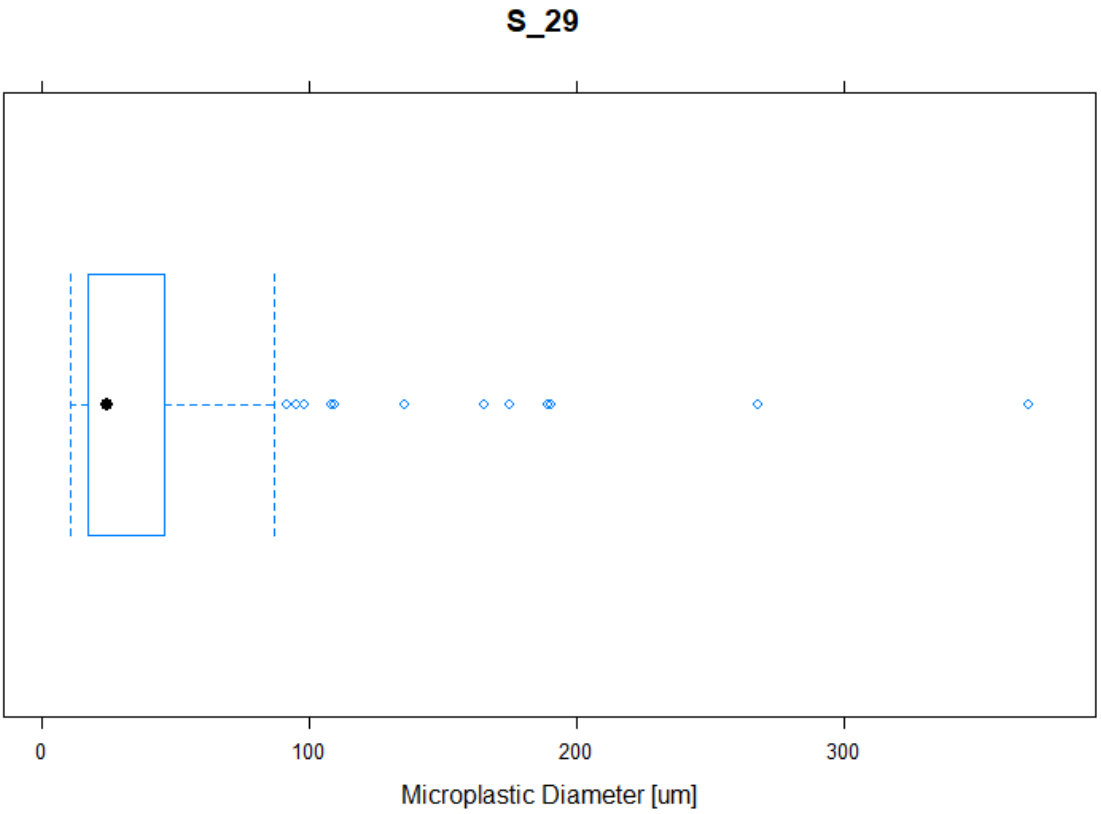
S_29
0
100
200
300
Microplastic Diameter [um]

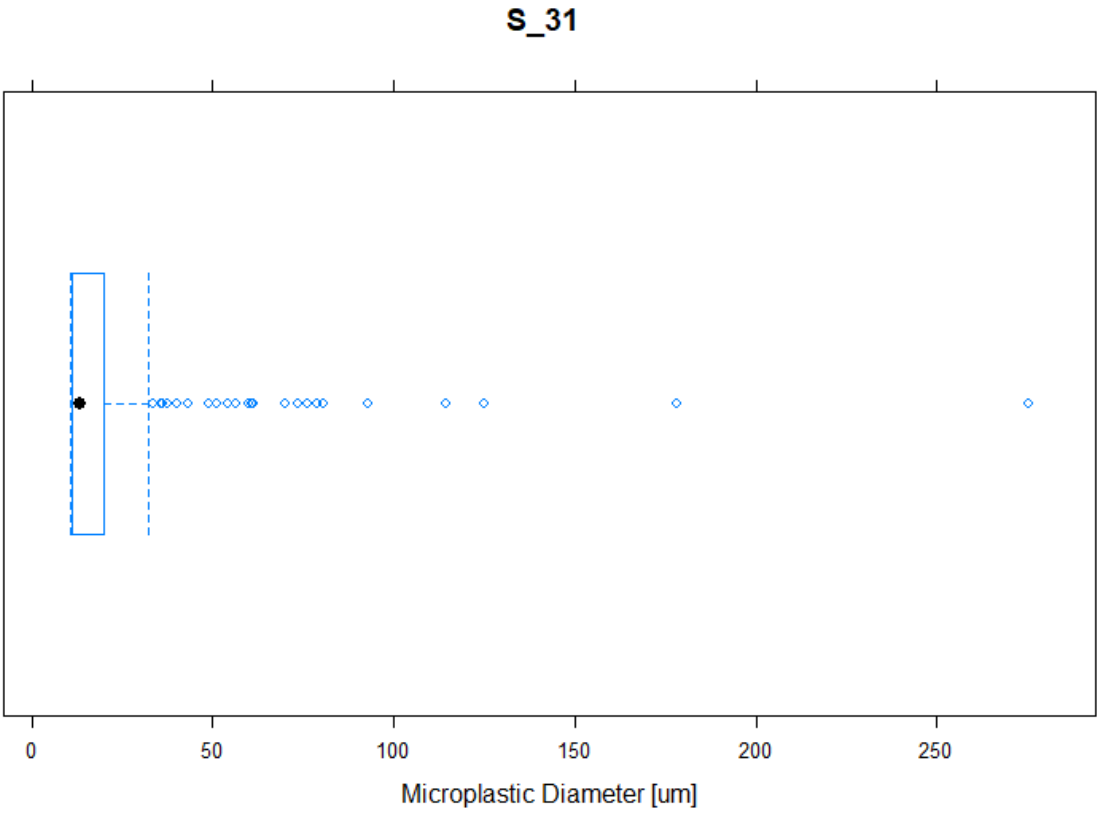
S_31
0
50
100
150
200
250
Microplastic Diameter [um]

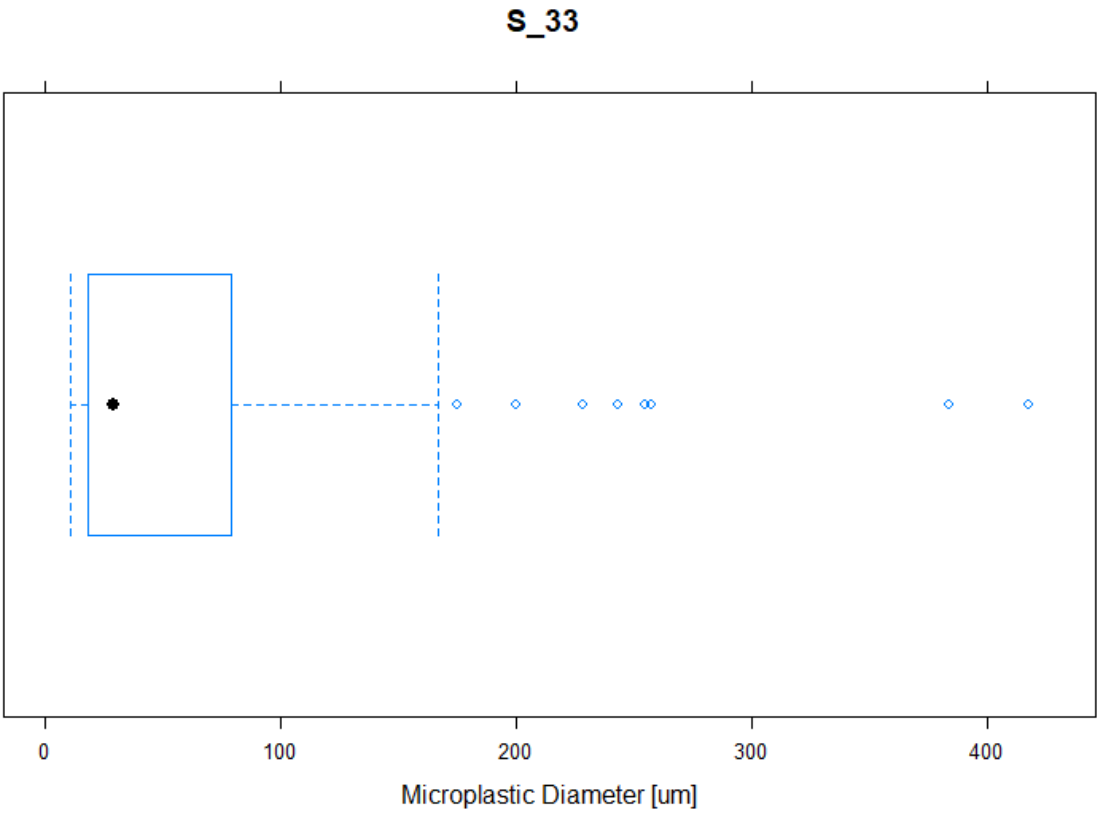
S_33
0
100
200
300
400
Microplastic Diameter [um]

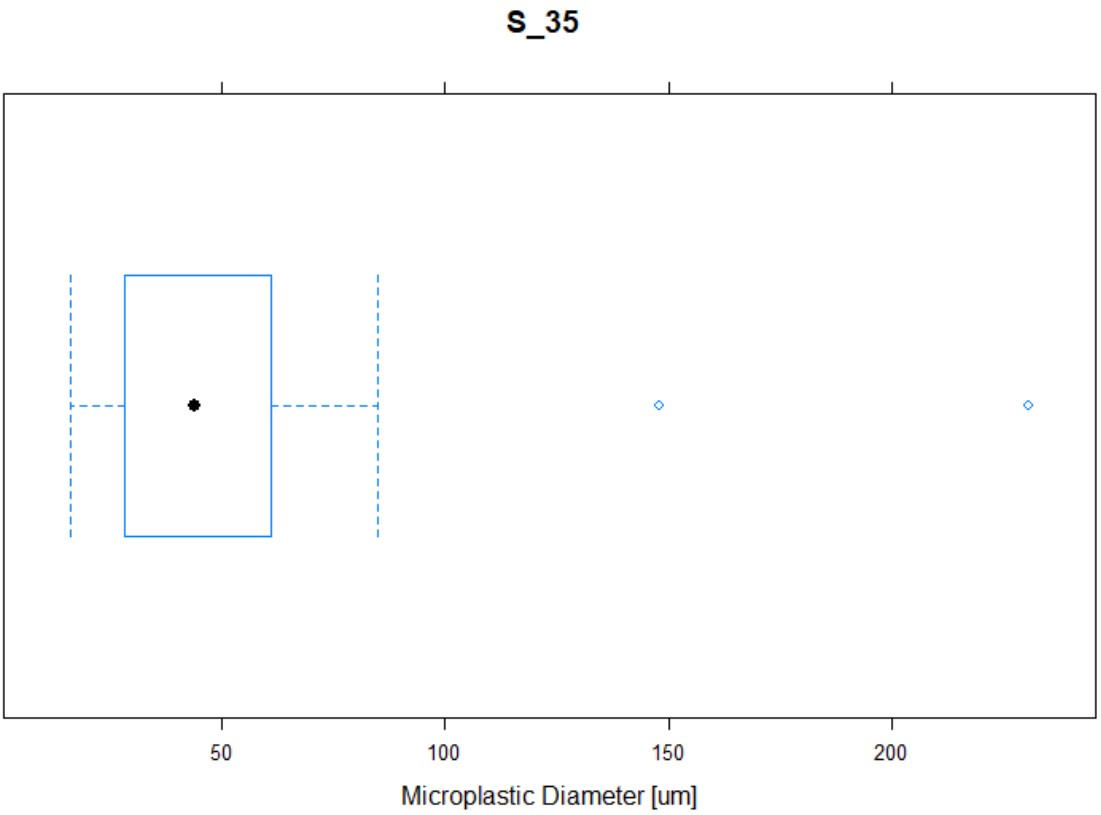
S_35
50
100
150
200
Microplastic Diameter [um]